



UNIVERSITEIT VAN PRETORIA
UNIVERSITY OF PRETORIA
YUNIBESITHI YA PRETORIA

Microstructural Evolution and its Influence on Mechanical Properties of Ti-Nb Binary Alloys

By

Lusanda Fikeni

12084426

Supervisor

Dr. KA Annan

Co-Supervisors

Dr. FK Mutombo

Prof. R. Machaka

Submitted in partial fulfillment of the requirement for the degree of
Master of Science (Metallurgy)

In the

Department of Materials Science and Metallurgical Engineering, Faculty of Engineering,
Built Environment & Information Technology

University of Pretoria
Republic of South Africa

[August 2021]

DEDICATION

To my late mother, Thobeka Fikeni.

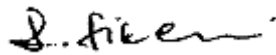
Your love, strength, guidance, and support made it possible for me to be where I am.

I am because you were.

Camagu Khanandana.

DECLARATION

I hereby declare that the dissertation submitted for the degree of Master of Science in Applied Science Metallurgy at the University of Pretoria, is my own original work and has not previously been submitted to any other institution of higher education.



Signed

Lusanda Fikeni,

Department of Materials Science and Metallurgical
Engineering

University of Pretoria

Date: 01 February 2021

PUBLICATIONS AND CONFERENCE PRESENTATIONS

1. Fikeni, L., Annan, K.A., Seerane, M., Mutombo, K., and Machaka, R., (2019), Development of a biocompatible Ti-Nb alloy for orthopaedic applications. Published IOP Conference Series: Materials Science and Engineering Vol. 655, doi:10.1088/1757-899X/430/1/012019.
2. Fikeni, L., Annan, K.A., Mutombo, K., and Machaka, R., (2021). Effect of Nb content on the microstructure and mechanical properties of binary Ti-Nb alloys. *Materials Today Proceedings*. Vol. 30, pp 913 – 917.
3. Fikeni, L., Annan, K.A., Mutombo, K., and Machaka, R., (2021). The influence of cooling methods after heat treatment on the microstructural evolution and microhardness of the Ti-13Nb alloy. Manuscript being prepared for submission to the *Journal of Material characterization*.

Candidate: Lusanda Fikeni

Supervisors: Dr. KA Annan, Dr. FK Mutombo and Prof. R. Machaka

Institution: University of Pretoria

Department: Materials Science and Metallurgical Engineering

Degree: M.Sc. (Applied Science) Metallurgy.

ACKNOWLEDGEMENTS

Throughout the research work and writing of this dissertation I have received a great deal of support and assistance; therefore, I would like to extend my sincere gratitude. Firstly, I would like to thank my supervisor, Dr. Kofi A. Annan, whose patient support, and expertise were invaluable throughout my journey of conducting and completing the master's project and most importantly the opportunity to further my studies. I would also like to thank my co-supervisors Prof Ronald Machaka and Dr Kalenda Mutombo for their valuable guidance and support throughout my studies. I would also like to acknowledge the financial support of the Advanced Materials Initiative (AMI), the Department of Science and Innovation (DSI) South Africa, the Titanium Centre of Competence (TiCOC), and the Council of Scientific and Industrial Research (CSIR).

I would like to acknowledge my colleagues from the Advanced materials engineering, Materials Science & Manufacturing at CSIR. I would particularly like to thank my colleagues Lerato Raganya, Nthabiseng Moshokoa, Ntswaki Nyakane and Mandy Seerane from Prof. Ronald Machaka's research group. I would also like to acknowledge the academic, and technical support received from the University of Pretoria and the CSIR.

In addition, I would like to thank my family and friends for their encouragement, unwavering support, counsel, and their ever always ready sympathetic ear.

ABSTRACT

Metallic biomedical implants that are currently used for orthopedic applications have shown biological and biomechanical incompatibilities. The first-generation titanium alloys that are currently commercially used are CP-Ti and Ti-6Al-4V. However, these alloys have higher elastic moduli with CP-Ti and Ti-6Al-4V 110 GPa compared to that of the human bone which ranges from 4-30 GPa. The higher elastic modulus causes the stress shielding effect which leads to bone absorption and causes implant loosening and eventually implant failure. The alloying elements aluminum and vanadium of Ti-6Al-4V have been reported to cause allergic reactions in the human body and have lasting detrimental effects to the body. Therefore, development of new biomedical metallic alloys specifically of β -titanium alloys has been underway that are biocompatible and have suitable combination of mechanical properties. This study aimed at developing a biocompatible β -Ti-Nb alloy with improved mechanical properties for different applications. The effect of the β -stabilising element Nb is specifically investigated on the microstructural evolution and the mechanical properties of the Ti-Nb alloys. The influence of heat treatment and the use of different cooling mediums was evaluated on the Ti-Nb alloys.

Ti-Nb alloys with a composition range of 1-49 wt.% were fabricated using the vacuum arc remelting process using CP-Ti and Nb as starting materials. The as-cast and solution-treated Ti-Nb alloys were characterized for microstructures and phases formed with OM, SEM-EDX and XRD. The phase transformations that occurred as the as-cast alloys were heated from room temperature up to the β -phase field were determined using the DSC. The

Vickers microhardness and tensile properties of the as-cast Ti-Nb alloys were determined to demonstrate the effect on Nb on the mechanical properties.

The microstructures of the as-cast Ti-Nb alloys evolved from α -lamellar to a mixture of α - α' -and α'' -martensite, and the metastable β -phase and then the metastable β -phase was fully retained as the Nb content increased. The microhardness, 0.2% yield strength and ultimate tensile strength of the as-cast alloys showed a general increase with increasing Nb content before it decreased for the alloys with high Nb content. However, the Ti-49Nb alloy had the highest UTS and 0.2% YS and the lowest elongation, exhibiting good strength but poor ductility behavior. The addition of the β -stabilising Nb element lowered the Young's modulus as its content was increased with Ti-35Nb alloy having the lowest elastic modulus of 65.2 GPa. The slow cooling of the Ti-Nb alloys after solution treatment led to the formation of the α -phase for low Nb content alloys and the martensitic phases for high Nb content alloys. Whereas rapidly cooling led to increase in stabilising the metastable β -phase at room temperature from Ti-13Nb alloy and produced a fully martensitic microstructure for Ti-7Nb alloy. The different cooling rates did not alter the phases obtained by Ti-1Nb alloy however the α -lamellar microstructure was refined as the cooling rate increased. The air-cooled samples showed the maximum microhardness due to the refined microstructures and martensitic phases formed. The metastable β -phase retained in water-quenched Ti-Nb alloys led to a decrease in hardness.

The Ti-Nb alloys exhibited lower Young's modulus compared to the conventionally used titanium alloys and good mechanical strength. The Ti-35Nb alloy can be considered as a potential biomedical implant due to its lower Young's modulus that is comparable to that of the human bone.

TABLE OF CONTENTS

DEDICATION	i
DECLARATION	ii
PUBLICATIONS AND CONFERENCE PRESENTATIONS	iii
ACKNOWLEDGEMENTS	iv
ABSTRACT	v
LIST OF FIGURES	ix
LIST OF SYMBOLS AND ABBREVIATIONS	xi
CHAPTER 1. INTRODUCTION	1
1.1 Background and Motivation	1
1.2 Problem Statement	3
1.3 Aim and Objectives of the Study	5
1.4 Scope	5
1.5 Organization of this Dissertation	6
CHAPTER 2. LITERATURE REVIEW	7
2.1 Biomedical Implants	7
2.2 Beta-titanium alloys	11
2.3 Ti-Nb alloys	13
2.4 Vacuum arc remelting process	17
2.5 Heat treatment of Ti-Nb alloys	18
CHAPTER 3. The experimental procedure	19
3.1 The starting materials	21
3.2 Powder characterization	21
3.3 Powder compaction	22
3.4 Vacuum arc remelting	23
3.5 Heat treatment	24
3.6 Metallographic sample preparation	25
3.7 Metallographic and phase characterization	25
3.8 Mechanical testing	27
CHAPTER 4. RESULTS	29
4.1 Characterization of the starting powders	29
4.2 Characterization of the Ti-Nb alloys	33
4.2.1 Microstructural analysis of the as-cast and solution-treated Ti-Nb alloys	33
4.2.2 Phase analysis of the as-cast and solution-treated Ti-Nb alloys	41
4.2.3 Phase transformations of the as-cast Ti-Nb alloys	46

4.2.4	Vickers micro-hardness of the as-cast and solution-treated Ti-Nb alloys	50
4.2.5	Tensile properties of the as-cast Ti-Nb alloys	53
CHAPTER 5. Discussion		57
5.1	Characterization of the starting elemental powders	57
5.2	Characterization of the Ti-Nb alloys	58
5.2.1	Microstructural analysis of the as-cast and solution-treated Ti-Nb alloys	58
5.2.2	Phase analysis of the as-cast and solution-treated Ti-Nb alloys	62
5.2.3	Thermal analysis of the as-cast Ti-Nb alloys	64
5.2.4	Micro-hardness of the as-cast and solution-treated Ti-Nb alloys	66
5.2.5	Tensile properties of the as-cast Ti-Nb alloys	70
CHAPTER 6. CONCLUSIONS		73
6.1	Conclusions	73
6.2.	Recommendations	75
REFERENCES		77

LIST OF FIGURES

Figure 2.1: Ti-Nb equilibrium phase diagram ²⁷	14
Figure 2.2: Calculated T ₀ and M _s curves in Ti-Nb phase diagram ²⁵	15
Figure 3.1: The overview of the experimental procedure followed in the study.	20
Figure 3.2: The hydraulic press machine (a) and the Ti-Nb green compact (b).	22
Figure 3.3: The button arc vacuum furnace.	24
Figure 3.4: The dimensions of the tensile specimen that was cut from Ti-Nb ingot and tested for tensile properties.	27
Figure 3.5: a) The Ti-Nb ingot from which the tensile specimens were cut b). image of machined tensile test specimen.	28
Figure 4.1: The particle size distribution curves of (a) CP-Ti powder and (b) Nb powder and the SEM micrographs of (c) CP-Ti powder and (d) Nb powder.	30
Figure 4.2: The XRD patterns of the starting powders of (a) titanium and (b) niobium. .	31
Figure 4.3: The stable phases of Ti-Nb are shown on the phase diagram of Ti-Nb calculated using Thermocalc and the Ti-Nb compositions.	32
Figure 4.4: The optical micrographs of (a) Ti-1Nb, (b) Ti-7Nb, (c) Ti-13Nb, (d) Ti-28Nb, (e) Ti-35Nb and (f) Ti-49Nb as-cast alloys.	34
Figure 4.5: The SEM back-scatter micrographs of (a) as-cast, (b) water-quenched, (c) air-cooled and (d) furnace-cooled microstructures of Ti-1Nb alloy.	35
Figure 4.6: The SEM back-scatter micrographs of (a) as-cast, (b) water-quenched, (c) air-cooled and (d) furnace-cooled microstructures of Ti-7Nb alloy.	36
Figure 4.7: The point and shoot analysis showing composition of the microstructures of (a) Ti-7Nb-FC and (b) Ti-13Nb-FC after solution treatment.	37
Figure 4.8: The SEM back-scatter micrographs of (a) as-cast, (b) water-quenched, (c) air-cooled and (d) furnace-cooled samples of Ti-13Nb alloy.	38
Figure 4.9: The SEM back-scatter micrographs of (a) as-cast, (b) water-quenched, (c) air-cooled and (d) furnace-cooled samples of Ti-28Nb alloy.	39
Figure 4-10: The SEM back-scatter micrographs of (a) as-cast, (b) water-quenched, (c) air-cooled and (d) furnace-cooled samples of Ti-35Nb alloy.	40
Figure 4.11: The SEM back-scatter micrographs of (a) as-cast, (b) water-quenched, (c) air-cooled and (d) furnace-cooled samples of Ti-49Nb alloy.	41
Figure 4.12: The XRD patterns of the as-cast Ti-Nb alloys.	42
Figure 4.13: The XRD patterns of the as-cast, furnace-cooled (FC), air-cooled (AC) and water-quenched (WQ) samples Ti-1Nb and Ti-7Nb alloys.	44
Figure 4.14: The XRD patterns of the as-cast, furnace-cooled (FC), air-cooled (AC) and water-quenched (WQ) samples Ti-13Nb and Ti-28Nb alloys.	45
Figure 4.15: The XRD patterns of the as-cast, furnace-cooled (FC), air-cooled (AC) and water-quenched (WQ) samples Ti-35Nb and Ti-49Nb alloys.	46
Figure 4.16: The DSC scans of the as-cast Ti-Nb alloys illustrating the endothermic and exothermic reactions as the alloys were heated from room temperature up to 1200 oC, (a) DSC curves for the Ti-Nb alloys and (b) DSC curves for Ti-13Nb, Ti-28Nb and Ti-35Nb alloy.	48
Figure 4.17: The Vickers micro-hardness of the as-cast Ti-Nb alloys.	51

Figure 4.18: The Vickers micro-hardness of the as-cast, water-quenched (WQ), air-cooled (AC) and furnace-cooled (FC) Ti-Nb alloys.	53
Figure 4.19: The stress-strain curves of the as-cast Ti-Nb alloys.....	54
Figure 4.20: The tensile properties of the as-cast Ti-Nb alloys the (a)0.2% yield strength and (b) ultimate tensile strength.....	55
Figure 4.21: The tensile properties of the as-cast Ti-Nb alloys (a) elastic modulus and (b) elongation.....	56

LIST OF SYMBOLS AND ABBREVIATIONS

SYMBOL	DESCRIPTION
AC	Air cooled
α	Alpha
Al	Aluminum
atm	Standard atmosphere
α'	Hexagonal martensite
α''	Orthorhombic martensite
β	Beta
BCC	Body centered cubic crystal structure
Co	Cobalt
Cr	Chromium
CP-Ti	Commercially pure titanium
°C	Degrees Celsius
DSC	Differential scanning calorimetry
EDX	Electron dispersive spectrometry
FC	Furnace cooled
GPa	Gigapascals
HCP	Hexagonal closed packed crystal structure
HF	Hydrofluoric acid
M_f	Martensitic finish temperature
M_s	Martensitic start temperature
MPa	Megapascals
MIM	Metal injection molding
Mo	Molybdenum
Ni	Nickel

Ni-Ti	Nitinol
Nb	Niobium
Nb ₂ O ₅	Niobium pentoxide
ω	Omega
OM	Optical microscopy
SEM	Scanning electron microscopy
Ta	Tantalum
Ti	Titanium
Ti-Nb	Titanium-Niobium
TiO ₂	Titanium oxide
VAR	Vacuum arc remelting
V	Vanadium
WQ	Water quenched
wt. %	Weight percent
XRD	Xray diffraction
Zr	Zirconium

CHAPTER 1. INTRODUCTION

The chapter details briefly the background and motivation of the study of the development of Ti-Nb alloys as candidates for biomedical alloys. The problem statement for the study has been given. The aim and objectives of the study are presented in this chapter as well as the scope and the organization of the dissertation.

1.1 Background and Motivation

Titanium and its alloys among the metallic biomaterials have been the most attractive due to their combined good properties, high strength, good corrosion resistance, biocompatibility and lower elastic modulus¹⁻³. The titanium element has low density which is approximately half of that of iron and cobalt that can be strengthened by thermomechanical processing and alloying⁴. Titanium and its alloys generally have good corrosion resistance due to the formation of the stable TiO₂ passive oxide film on their surface which re-passivate faster than the other biomedical implant¹. The commercial pure titanium (CP-Ti) and Ti-6Al-4V are the mostly used titanium alloys for implants due to their lower Young's modulus and good corrosion resistance compared to the stainless steel and cobalt-based alloys. Ti-6Al-4V is a first generation orthopedic $\alpha+\beta$ titanium alloy which has been used for total hip arthroplasties because of its good high specific strength^{3,5}.

Biomaterials are biocompatible natural or man-made materials that are used as implants to replace certain parts of a human body to restore lost form and assist in the function of the biological systems^{1,4}. Biomaterials are used for different applications such as total joint replacements for hips, knees and shoulders, spinal fixation devices, cardiovascular tents

and dental applications for therapeutic and diagnostic procedures to improve the quality of life and longevity of human beings ^{1,4,6}. Over the last three decades, metallic biomaterials that have been used include stainless steel, cobalt-chromium alloys, titanium-based alloys, and other specialized alloys ^{1,4}. These alloys have been used as metallic implants for medical applications due to their biocompatibility, corrosion resistance and relatively high strength ². However, stainless steel and cobalt chromium alloys have shown limitations such as corrosion fatigue, and they contain Ni, Co, Cr elements which cause biological toxicity when released in the human body ². These alloys also cause the stress shielding effect that leads to implant failure due to their higher Young's modulus compared to that of the lower elastic modulus of human bones ^{1,2,4}.

The predominantly used titanium alloy, Ti6Al4V has an elastic modulus of 110 GPa which is still higher than that of the human bone ². The Young's modulus of the human bone is between 4 GPa and 30 GPa, therefore implants with higher Young's modulus may cause the stress shielding effect ^{1,7}. The stress shielding effect is when the implant bears most of the mechanical load, shielding the bone from bearing the load required for it to maintain strength and healthy structure due to the high Young's modulus of the implant ^{1,7}. The higher elastic modulus of Ti-6Al-4V therefore prevents adequate transfer of stress to the adjacent bone and this prohibits bone formation and osseointegration leading to implant loosening and bone resorption ¹⁻³. The wear or corrosion of the protective oxide layer in implants leads to the release of the alloying element ions and their oxides which may cause adverse reactions in the body. The release of Ti-6Al-4V alloying elements such as aluminium and vanadium ions have shown to cause biological toxicity which causes aseptic loosening of the implant and this may even lead to revision surgery^{1,8,9}.

Beta-titanium alloys are widely studied and considered as the next potential biomedical implants due to their low Young's modulus, non-toxic β -stabilising elements, enhanced strength and fracture toughness and their excellent cold and warm formability^{4,8}. Titanium alloys have a range of possible microstructures depending on the alloying element composition and thermomechanical processing after fabrication. The Young's modulus is a materials property dependent on the phase of the titanium alloy; In Ti, the ω -phase has the highest Young's modulus with martensitic phases having relatively low Young's modulus and the beta-alloys with the lowest Young's modulus⁷. Beta-titanium binary alloys with niobium, molybdenum and tantalum as beta-stabilising alloying elements are being developed to lower the elastic modulus, enhance biocompatibility and corrosion resistance³. The biological toxicity and mechanical incompatibility of the currently used biomaterials that lead to implant failure thus require revision surgery and degenerative diseases such as arthritis and musculoskeletal disorders require the development of metallic biomaterials with high biocompatibility and suitable mechanical properties^{1,2}.

1.2 Problem Statement

The most commonly used Ti-based alloy is the two phase ($\alpha+\beta$) Ti-6Al-4V¹⁻³. The β -Ti alloys offer many advantages in terms of processing, mechanical properties, and low cost of fabricated components to the Ti-6Al-4V³. For medical applications Al and V are found to be biologically toxic as well as mechanical property mismatch of most used implants^{1,4-6}. However, there are melting difficulties, reproducibility problems and related phase transformation consequences for the β -phase Ti- alloys. The amounts of β stabilizing elements have been found to influence the structure and property of β – Ti alloys^{3,7}. The exact composition of elements such Nb as well as

the process route and its influence on the structure and mechanical properties have not been established.

It has been estimated that 90% of the population over the age of 40 suffers from human joints degenerative diseases to some degree ⁸⁻¹⁰. The number of total hip replacements is expected to rise by 174% (572 000) and total knee arthroplasties to increase by 673% (3.48 million procedures) and the revision surgeries are expected to increase by 137% and 607% for hip and knee revision surgery, respectively, between 2005 and 2030 ^{1,6,7}. The commonly used artificial biomaterials as implants for orthopedic applications are metals and polyethylene; with 70-80% being metallic biomaterials ^{2,7}. The currently used metallic biomaterials tend to fail due to mechanical property mismatch and biological toxicity. The poor corrosion and wear resistance and the toxic alloying elements are also found to cause aseptic loosening of the implant which also leads to implant failure ¹. Therefore, there is a need for long-lasting metallic implants that are biocompatible, have superior wear and corrosion resistance, high fatigue, and strength as well as low Young's modulus that is comparable to that of the human bone ^{1,10}. The development of second generation Ti-alloys that consists of β -titanium alloys has been done and is being continually explored. Beta-Ti alloys such as Ti-13Nb-13Zr, Ti-15Mo-5Zr-3Al and Ti-Nb-Zr-Ta (TNZT) alloys have proven to have lower Young's modulus than Ti-6Al-4V ⁶. The contribution of the content levels β -stabilizing Nb element have however not been established. Ti-Nb alloys are therefore promising materials for use as biomedical implants. As the content of Nb increases, several phases (α , α' , α'' , ω , and β) may nucleate in the Ti-Nb alloys. These phases directly influence the mechanical and functional properties of the alloys ^{11,12}. The aim of this work is, therefore, to study the influence of Nb as the β -stabilizing element in

the evolution of the microstructures as well as their effect on the mechanical properties of Ti-Nb binary alloys.

1.3 Aim and Objectives of the Study

The aim of this work is to study the effect of the beta-stabilizing niobium (Nb) alloying element on Ti-Nb alloys in development of a beta-titanium alloy. The research objectives followed in achieving the set aim were:

1. To determine the effect of the alloying element Nb on the microstructures of Ti-Nb alloys.
2. To determine the influence of Nb and its content on the tensile properties of Ti-Nb alloys.
3. Evaluate cooling methods after casting on Ti-Nb alloys for their microstructural evolution and microhardness.

1.4 Scope

The current study focuses on the effect of Nb on Ti-Nb alloys in development of a beta Ti-Nb alloy. The influence of Nb on the Ti-Nb composition ranging from 1 to 49 wt.% Nb on the microstructural evolution and tensile properties has been studied. The as-cast Ti-Nb alloys were fabricated using the vacuum arc remelting process after cold compaction of the powders with their respective compositions. The Ti-Nb alloys were solution treated and furnace cooled, air cooled and water quenched. The as-cast and solution-treated alloys were characterized for microstructures and phases using optical microscope, scanning electron

microscope and X-ray diffraction; the tensile properties were determined using tensile testing.

1.5 Organization of this Dissertation

This dissertation consists of six chapters. Chapter one gives the overall background, motivation and focus of this research study. Chapter two contains the literature review on the application of Ti alloys, in-depth understanding of Ti-Nb alloys, processing and heat treatment techniques of these alloys. The details of the experimental procedures used in this study are discussed in chapter three. The results and discussion is divided into two chapters, which are chapter four and five. Chapter four, presents characterization and mechanical results of Ti-Nb alloys. Chapter five contains thorough discussion of the results. Conclusions and recommendations obtained from this research study are given in Chapter six.

CHAPTER 2. LITERATURE REVIEW

The chapter details through literature review the advantages and shortcomings of the metallic implants that have been used for biomedical applications. The review of the beta-titanium alloys as potential implants for biomedical applications. The research that has been conducted on Ti-Nb alloys as potential biomedical implants due to their lower Young's modulus and biocompatibility has been reviewed. The vacuum arc remelting process was used as the fabrication process. The effect of heat treatment on the microstructures and mechanical properties of titanium alloys has also been reviewed.

2.1 Biomedical Implants

Metallic biomedical implants have been used since the 19th century in an approach to meet the demands for bone repair specifically for internal fracture fixation of long bones ⁴. Metallic implants have been predominantly used for orthopedic applications since, for permanent implants such as total joint replacements as well as temporary devices such as bone plates and screws ^{1,4}. The metallic implants that have been used are stainless steel, cobalt-based alloys, titanium-based alloys and specialized alloys such as NiTi and alloys of Mg for orthopedic applications ⁴. The currently used metallic biomaterials have led to implant failure due to biological toxicity, mismatch of the Young's modulus because it is higher than that of the human bone and due to low corrosion and wear resistance after long-term use ¹.

Stainless steels are a group of iron-based alloys that contain chromium (11-30wt%) and varying amounts of nickel ¹. The 316L stainless steel has shown relatively good

biocompatibility, however CoCrMo and titanium alloys are more biocompatible than the stainless steel because the stainless steels have increased corrosion rates and nickel and chromium ions have been reported to be toxic and carcinogenic ⁴. The wear resistance of 316L austenitic stainless steel is also relatively poor, the wear debris has led to allergic reactions in surrounding tissue therefore stainless steels are not suitable for permanent implantation⁴. The stainless steel has a Young's modulus of 210 GPa which is higher than that of the human bone and therefore likely to cause stress shielding effect leading to implant failure ^{1,11-13}. Premature failure of stainless steel implants has been reported which can occur from several months to several years after implantation due to fatigue failure caused by corrosion or fretting failure ⁴.

Cobalt-chromium alloys have superior corrosion and wear resistance than the stainless steels due to the high chromium content that forms a passive oxide layer in the human body environment ^{2,4}. However, the cobalt-chromium alloys also have high Young's modulus ranging from 220–230 GPa, which is much higher than that of cortical bone (20–30 GPa), the high Young's modulus results in uneven energy distribution ^{4,6}. The effect of the stress-shielding effect, wear debris and the inflammation caused by the toxic metal ions of Ni, Co and Cr released from cobalt-based alloys eventually leads to implant failure ⁴.

Titanium and its alloys have been used as biomaterials due to their high strength-weight ratio, good biocompatibility, corrosion resistance and good mechanical properties ^{4,10}. Titanium and its alloys have lower Young's modulus compared to the stainless steels and cobalt-based alloys, however, they have inferior wear resistance ^{4,12,14}. The first-generation titanium alloy, Ti-6Al-4V has a lower Young's of 110 GPa compared to stainless steels and cobalt-based alloys ¹⁰. However, the alloying elements V and Al have been

reported to cause adverse reactions which lead to cell death and long-term health problems^{4,13}. Development of second-generation titanium alloys is now the focus for medical applications with non-toxic elements such as Ta, Nb and Mo with even lower Young's modulus.

It is important for a metallic implant to have the following requirements for a successful long-term service for orthopedic applications. That is good biocompatibility, suitable mechanical properties such as high strength, good corrosion and wear resistance, low elastic modulus and Osseo-integration^{1,10}. A biomedical implant is designed to be in intimate contact with the living tissue, therefore, it is important that it does not cause any harmful effects to the human body. Biocompatibility of a biomaterial depends on the specific medical application; however, it includes both the biological and mechanical compatibilities to the host. Therefore the biocompatibility of a metallic implant includes the chemical interactions of the implant with the host's physiological system that is the toxicities of the metal ions to the cells and tissues and the physical impacts of the implant on the surrounding tissue that is the mechanical properties compatibility⁴. The biocompatibility of the implant is measured by the reaction the human body has to the material after implantation¹.

The mechanical properties of the implant are very important for the function of the biomaterial and its longevity in the human body. Mechanical properties such as tensile strength, fatigue strength, ductility and the Young's modulus of the material are some of the most important properties of the material to be considered for an orthopedic implant⁶. The Young's modulus of the biomaterial is expected to be close to that of the bone which varies from 4-30 GPa depending on the type of bone^{1,2,13}. Mismatch in the elastic modulus

of the bone and the implant causes the stress-shielding effect which leads to bone resorption and then implant failure ^{1,6}. The fatigue strength of the biomedical implant is an important mechanical property for orthopedic applications as the material will be used under fatigue conditions ¹⁰.

The human body has different conditions from the ambient conditions and different parts of the body have different pH values and oxygen concentrations, therefore metal implants may react differently inside the human body than in ambient conditions. The body fluids contain aqueous fluids, proteins, trace elements and saline solutions of sodium and chloride ions with pH values 7.2-7.4 at 37 °C at atm pressure ⁴. Corrosion of an implant depends on its corrosion resistance, biological environment conditions, mechanical factors and electromechanical effects ⁷. High corrosion and wear resistance of the biomaterial is very important as released metal ions and wear debris may cause inflammation and allergic reactions that would lead to implant loosening ¹. However, surface coatings such as hydroxyapatite, titanium, calcium silicate, Al₂O₃, ZrO₂, TiO₂, TiN, TiC and TiCN, can be used to improve the wear and corrosion resistance of the implant ¹⁴.

Corrosion of an implant depends on its corrosion resistance, biological environment conditions, mechanical factors and electromechanical effects⁷. The composition and thickness of a stable passive oxide film formed on the surface of the implant increases their corrosion resistance and minimizes the release of metal ions ⁴. Wear damage causes aseptic loosening of the implant due to inflammation and adverse reactions. The wear debris attracts immune system macrophages which recognise the particles as foreign bodies however these particles tend to kill the macrophages releasing enzymes and metabolites which causes a very acidic surrounding environment which leads to the loosening of the

implant⁴. The corrosion and wear resistance of the implant is dependent on the stability of the oxide surface films^{1,4}.

Integration of the implant with the bone is very important for new cell and tissue growth to occur for long-term implantation to occur. Osseo-integration is the process of new bone healing and the formation, growth and differentiation of new bone cells on the implant surface¹. It is very important for the implant to have the appropriate surface chemistry and roughness in order to integrate well with the surrounding bone and tissue^{1,2}. Failure of the implant to integrate with its surroundings may occur due to inflammation and micromotions of the implant which causes the formation of fibrous tissue and all of this promotes loosening and rejection of the implant^{1,4}. The implant surface can be improved through development of porous surface, oxides coating and reduction of grain size by heat treatment of the surface to ensure successful Osseo-integration⁴.

2.2 Beta-titanium alloys

Pure titanium is an allotropic metal that has two different crystal structures, a low temperature hexagonal close packed crystal structure (α -phase) and a high temperature body centered cubic crystal structure (β -phase)^{1,15,16}. The temperature at which α transforms to β is called the β -transus temperature and addition of alloying elements to Ti may alter this temperature leading to a range of phases and mechanical properties¹⁶. The titanium alloys can be classified as α alloys, near- α alloys, α - β and β alloys based on their microstructures^{4,17-20}. Alloying elements can be either classified as an α -stabilizer or a β -stabilizer depending on their effect on the transformation temperature between α - and β -phases^{4,15,21-23}. If an alloying element decreases the transformation temperature thus

stabilizing the β -phase at lower temperature, then it is classified as a β -stabilizer and if it increases it thus stabilizing the α -phase at higher temperature then it is an α -stabilizer. The β -titanium alloys are considered the second generation of titanium biomaterials, they are being developed due to their lower Young's modulus that is closer to that of the bone compared to the commercially used α - and $\alpha+\beta$ alloys^{14,24}. The high temperature β -phase can be fully retained at room temperature by alloying titanium with enough β -stabilizing element, suitable heat treatment and fast cooling from the β -phase field.

The beta-titanium alloys exhibit lower elastic modulus and better biocompatibility due to the alloying with β -stabilizing elements that are used compared to the commercially used $\alpha+\beta$ Ti-6Al-4V alloy for biomedical applications^{4,6,17}. The elastic modulus of the metastable β -titanium alloys such as Ti-13Nb-13Zr, Ti-15Mo-5Zr-3Al and Ti-12Mo-6Zr-2Fe has been reported to range from 74 to 88 GPa and that of the TNZT alloys ranges from 55-66 GPa^{6,25}. The reported elastic moduli of the metastable β -titanium alloys is much lower than that of Ti-6Al-4V which is 110 GPa and that of commercially pure titanium which is 102-104 GPa^{6,17}. Instead of lowering the Young's modulus by inclusion of β -phase stabilizing elements in the alloy, designing 3D porous structures with controlled geometry and architecture could also reduce the implant stiffness. Using finite elemental modelling, theoretical compressive Young's modulus of about 1.1 to 1.4 \pm 0.1 GPa were obtained for porous Ti6Al4V alloy^{18,26,27}. The β -titanium alloys have good ductility and toughness, good hot and cold formability however they exhibit low creep strength and poor wear resistance^{4,6}.

The corrosion resistance of a material is dependent on the passive film layer formed on the surface and the presence of the alloying elements and their oxides²⁸. The β -stabilizing

elements such as niobium, zirconium and tantalum have very highly stable oxides in the human body that are incorporated in the titanium-oxide passive film stabilizing it thus increasing the corrosion resistance of the titanium alloy ^{1,6}. The alloying elements Nb and Zr of the metastable β -titanium alloy Ti-13Nb-13Zr have shown to have highly stable passive layers ¹¹. In studies conducted by Eisenbarth *et al.* (2004) ⁸, the beta- stabilizing elements niobium, zirconium and tantalum displayed non-toxic behaviour and good compatibility with direct contact with cells and relatively good cell growth and mitochondrial activity ⁸. A low modulus β -titanium alloy TNZT has been reported to be effective in inhibiting bone atrophy, leading to good bone remodeling in a bone fracture model in an animal intramedullary rod and bone plate implantation study compared to Ti-6Al-4V and stainless steel ².

2.3 Ti-Nb alloys

Ti-Nb alloys have attracted major attention in biocompatible metallic biomaterials for biomedical applications research due to their non-toxicity and lower Young's modulus associated with the non-toxic β -stabilizing element ^{19,20}. Niobium (Nb) is a non-toxic element with strong β stabilizing effect in Ti alloys, increases corrosion resistance and improves biological properties which makes Ti-Nb based alloys attractive for implant application ^{13,21}. Biological evaluation of the β -stabilizing elements Nb, Ta and Zr have shown that these elements are less cytotoxic than Ti ²². Alloying Ti with the β -stabilizing element Nb leads to a transformation of the metastable phases α' - and α'' -martensite, ω - and β -phase.

In the Ti–Nb equilibrium phase diagram as shown in Figure 2.1, two stable phases exist namely the BCC β and HCP α . Pure α Ti - phase is stable up to 882°C and β Ti - phase is stable between 882°C to 1670°C. The α to β transus temperature (882°C) decreases with addition of beta stabilizing elements (Nb, Mo, Ta) while the β phase stability increases. Depending on the content of β phase stabilizer and heat treatment conditions, α_1 (hexagonal), α_{II} (orthorhombic) and ω (hexagonal) metastable phases may form ²³.

The phase transformations taking place in annealed Ti-Nb alloy during rapid quenching from the β phase field are shown in Figure 2.2. Martensitic α_1 – phase form at low Nb contents of about 7.2 at. % (13.3 wt%) while at contents of 25.5 at. % (40.4 wt%) α_{II} – phase forms^{24–26}. At composition range of 14.3 and 25.5 at. % Nb and martensite start temperature Ms-curve is below the ω -start curve Ω_s , the α_{II} -martensite forms if rapidly quenched and ω -phase will form if slowly cooled ²⁵.

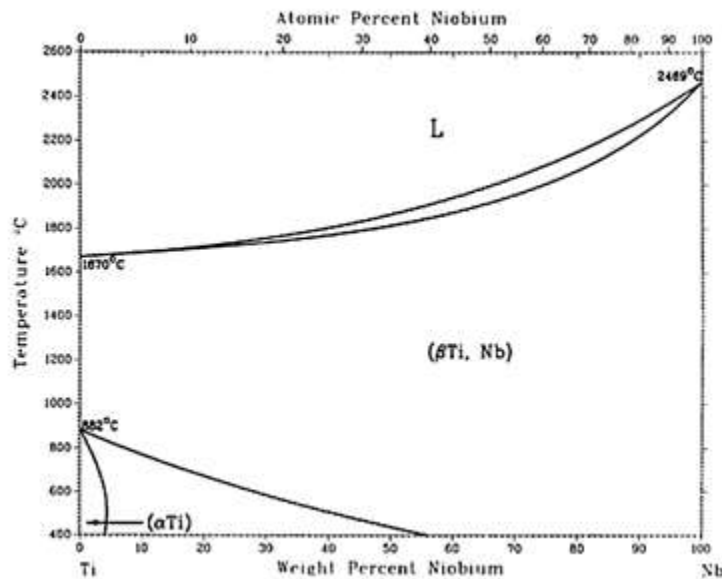


Figure 2.1: Ti-Nb equilibrium phase diagram ²⁷.

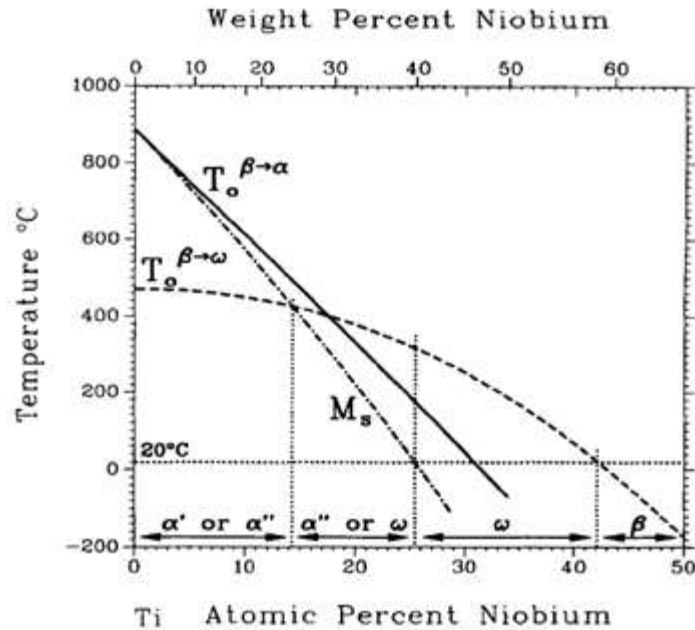


Figure 2.2: Calculated T_0 and M_s curves in Ti-Nb phase diagram²⁵.

The martensitic transformation from α' to α'' occurs at a critical alloying element content for beta-titanium alloys^{28,29}. The transformation of the α'' -martensite is preferred over the α' -martensite formation at high Nb content and it has been reported to occur at 9.3 to 17.7 wt.% Nb^{29,30}. The martensitic temperature (M_s) of binary Ti-Nb alloys decreases with increasing temperature and becomes lower than the room temperature when the Nb content is higher than 25.5 at.%³¹ for the β -phase to be retained. The Nb-element as a β -phase stabilizer increases the β/α ratio whilst maintaining good mechanical properties¹⁹. The Nb content has to be at least 35-40 wt.% for the β -phase to be completely retained and stabilized in Ti-Nb alloys¹⁹. Kikuchi³² reported in their study of Ti-(2-30 wt.%)Nb alloys that the phases obtained evolved from the α -phase into a mixture of the martensitic phases

and the β -phase was retained in the Ti-30Nb alloy along with the precipitation of the ω -phase³².

The Young's modulus of the Ti-Nb alloys is dependent on the Nb content as the alloys are being quenched from the β -phase field due to the phase compositions that transform in the alloy²⁹. The formation of the ω -phase in Ti-Nb alloys imposes a problem for the mechanical properties as it hardens the material and makes it brittle whilst it increases the Young's modulus^{33,34}. The Young's modulus of Ti-Nb alloys with a composition of 35-50 wt.% has been reported to be low with it ranging around 60 GPa³⁵. Zhao¹³ investigated Ti-Nb alloys with composition of 10-22 wt.%Nb using MIM technique. It was found that the Young's modulus and elongation decreased as the Nb content increased whilst the strength increased¹³. Whereas, the hardness of Ti-Nb alloys has been found to increase with increasing Nb content as the phases evolve from the α -phase into the martensitic and β -phase composition; the presence of the ω -phase further hardens the alloys before a decrease occurs as the β -phase is fully retained^{32,36,37}.

Furthermore, the doping of Nb in Ti based alloys was found to increase the corrosion resistance as compared to CP-Ti. This is due to the spontaneous formation of stable Nb oxides (Nb_2O_5) on the TiO_2 passive film, strong metal-metal bond strength and the lower dissolution of the Nb^{1,19}. Kim³⁸ reported insignificant metal ion release (<0.01lg/ml) when the Ti-Nb alloy was immersed in Hank's solution for 10-50 days. However, few metal ions (0.06– 0.07lg/ml) were observed in lactic acid solution (0.1%) after 50 days^{19,38}.

2.4 Vacuum arc remelting process

The Ti-Nb alloys have been manufactured using different processing techniques such as powder metallurgy, metal injection molding and casting^{13,36}. The Vacuum Arc Remelting (VAR) process is used for the production of high purity and homogeneous superalloys (such as titanium and zirconium alloys) with high melting points and oxygen sensitivity³⁹⁻⁴¹. The vacuum arc remelting process has been used as a refining process but now it is also being used as a principal ingot production process^{39,42}. The heating and melting of the metal alloy is established by the metal vapor electric arc that forms between a consumable electrode acting as a cathode and the molten pool of the ingot acting as an anode which solidifies in a water-cooled copper hearth⁴¹. In the process of vacuum arc remelting the compact Ti with the appropriate alloying elements is melted in what is called the primary melt in VAR furnace before it is remelted to promote chemical homogeneity⁴⁰. Titanium has a high affinity and solubility for oxygen as an interstitial element; both titanium and niobium suffer oxidation at high temperatures which affects the materials ductility at room temperature^{15,43}. The vacuum arc remelting process includes the interactions of the electromagnetic flow and heat transfers processes⁴⁴. The vacuum arc remelting process offers relatively pure ingots due to the protective vacuum, the high temperature caused by the electric arc melting and solidification in a water-cooled mold⁴³. The vacuum arc remelting process uses a consumable or a non-consumable electrode and a water-cooled mold for the production of the titanium alloy ingots⁴⁴.

2.5 Heat treatment of Ti-Nb alloys

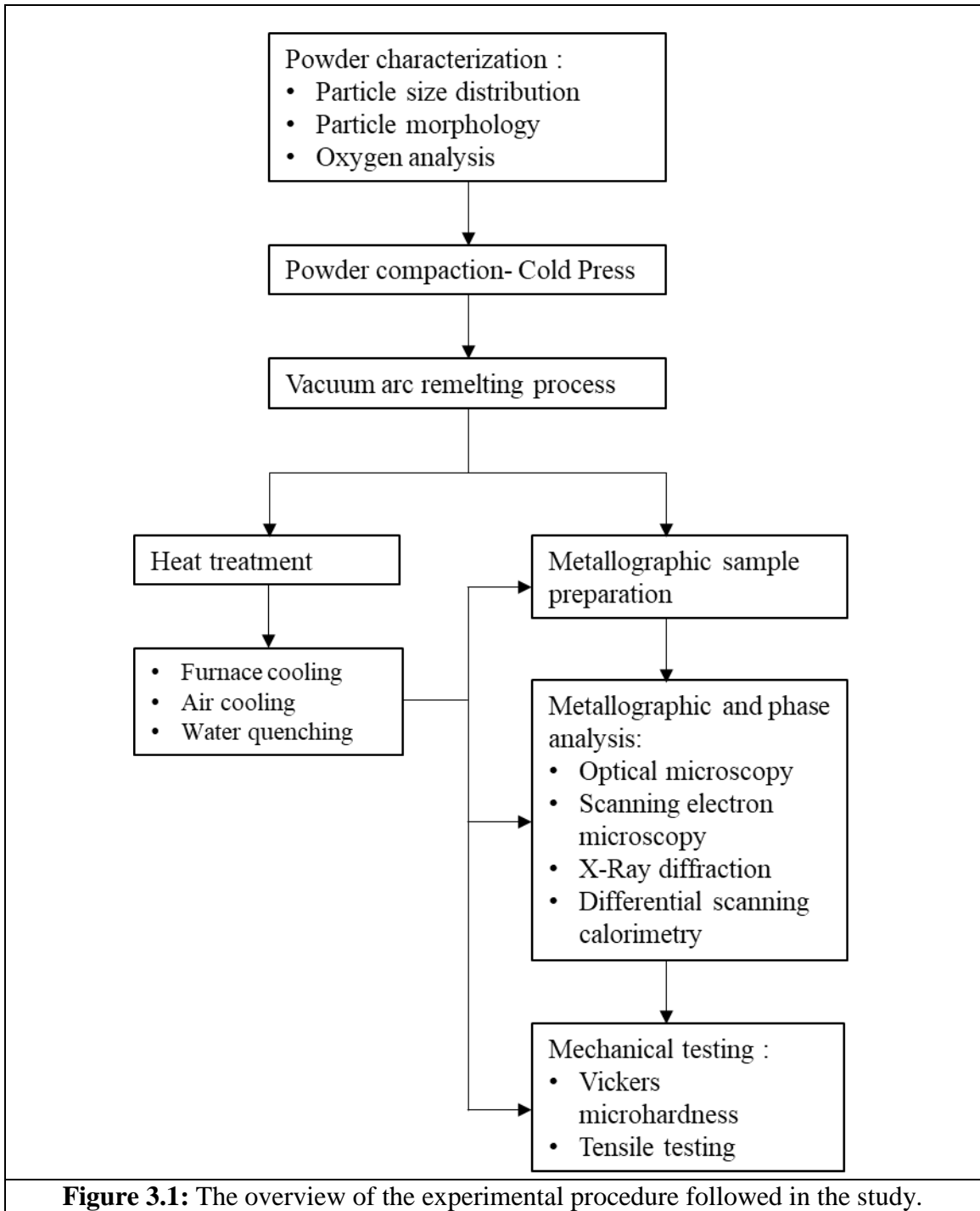
Suitable heat treatment and thermo-mechanical processing can be applied to beta-titanium alloys to produce the desired mechanical properties and lower Young's modulus. The microstructures that transform when Ti-Nb alloys are cooled from solution treatment from the β -phase field depend on the cooling rate and the heat treatment temperature²¹. When metastable β -titanium alloys are rapidly cooled from the beta-phase field, the hexagonal α' - and orthorhombic α'' -martensite are transformed³⁰. The martensitic phases transform and the metastable β -phase can be retained when Ti-alloys are rapidly cooled after heat treatment depending on the β -stabilizing element content¹⁶. The cooling rate from the heat treatment temperature determines the colony size, the width of the α -lamellar within the β -grains as well as the extent of the of the continuous α -layers at the β -grain boundaries⁴⁵. When the β -stabilizing element content is high and the sample is rapidly cooled from the β -phase field, the β -phase can be fully retained²¹. The metastable ω -phase can precipitate when Ti alloys are water quenched after heat treatment and the presence of the ω -phase of the alloys hardens the material and causes embrittlement^{30,33}.

Solution treatment of β -titanium alloys in the beta-phase field and rapid cooling leads to the decrease in elastic modulus however it also decreases its mechanical strength³⁰. In a study where a Ti-Nb alloy was solution treated and cooled with different cooling rates exhibited a range of phase compositions which showed a decrease in the Young's modulus as the cooling rates increased³⁵. The β -titanium alloys can be strengthened by applying appropriate heat treatment processes such as aging that lead to the transformation of the α -phase from the metastable ω -phase and α'' -martensite^{30,46}.

CHAPTER 3. THE EXPERIMENTAL PROCEDURE

The chapter details the experimental work and characterization techniques undertaken to meet the objectives and achieve the aim of this study. The starting materials and their characterization are described. The processes used to fabricate the Ti-Nb alloys, cold compaction, vacuum arc remelting and the post-processing heat treatment of the alloys are presented in this chapter. The metallographic process and tensile testing procedures followed in the current work are also explained.

Figure 3.1 presents a general overview of the various experimental steps followed in the study.



3.1 The starting materials

The starting elemental powders used in this work were titanium hydride-dehydride (99, 8 % purity) manufactured by Baoji Lihua Co. Ltd and Niobium (99, 8 % purity) by Industrial analytical (Pty) Ltd. The particle size of the titanium was reported by the manufacturer to be -150 μm and the particle size distribution of niobium was 1-5 μm .

3.2 Powder characterization

The starting elemental powders were analyzed for particle size distribution, oxygen content and particle morphology. The particle size distribution of the powders was done using the Microtrac Bluewave particle size analyzer. The morphology of the powder particles was analyzed using the Jeol JSM-6510 Scanning Electron Microscopy (SEM) equipped with electron dispersive spectrometry (EDX). The powder was set onto a carbon conductive tape on the sample holder. The backscatter electron and secondary electron imaging signals on the SEM were used for the analysis. The accelerating voltage that was used for analysis was 20 kV. The oxygen content of the powders was measured using the ELTRA ONH 2000 analyzer, which uses the inert gas fusion method. The process involved melting the sample in the furnace and measuring the oxygen content from the produced carbon dioxide by non-dispersive infrared cells. The mass of the sample analyzed was 100 mg and the sample carrier used was a graphite crucible. The process was repeated three times and an average of three measurements reported.

The phase diagram of Ti-Nb was calculated using Thermocalc. The phase diagram was calculated to showcase the stable phases that are obtained in the alloys as the Nb content

increases from 0 to 100 wt.%. The phase diagram was calculated over a temperature range of 0 to 2500 °C.

3.3 Powder compaction

The starting titanium and niobium contents were prepared with varying contents of Ti-1Nb, Ti-7Nb, Ti-13Nb, Ti-28Nb, Ti-35Nb and Ti-49Nb. The Ti-Nb alloy powders were cold compacted using a manually controlled hydraulic press machine shown in Figure 3.2(a). A cylindrical die fitted with a lower punch was loaded with the powder and then closed with a top punch. A pressure ranging between 500-800 MPa was applied manually to compact the powder at room temperature. The top punch was removed from the die assembly and then a suitable bushing was used to eject the green compact that is shown in Fig. 3.2(b).

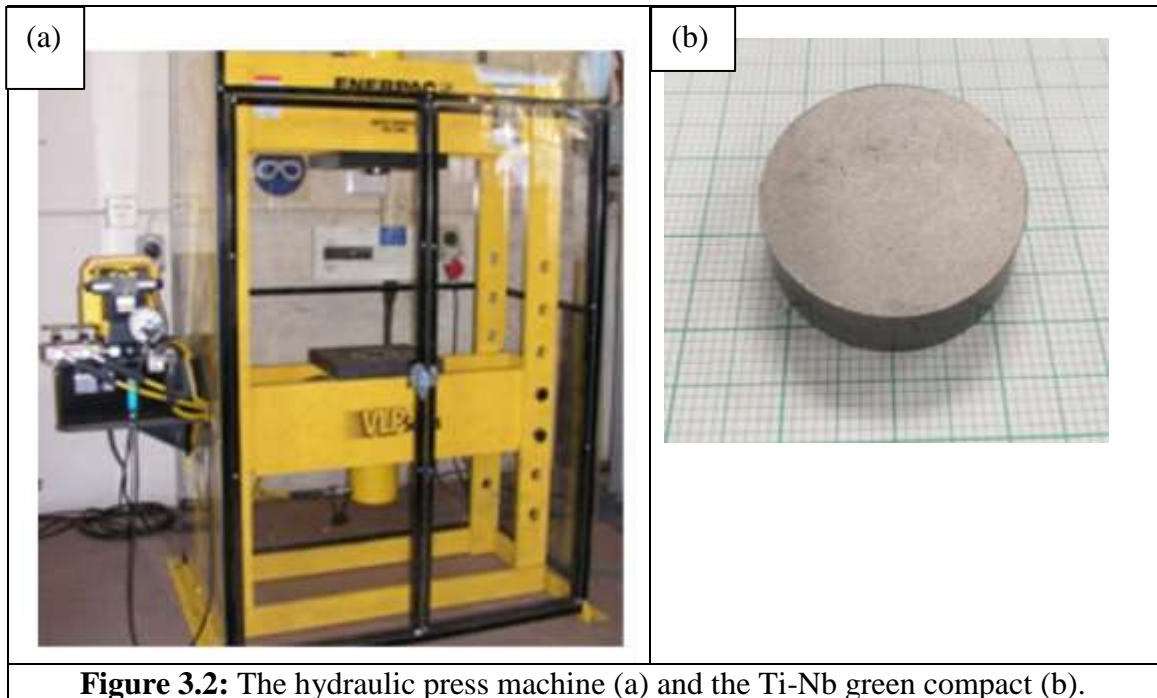


Figure 3.2: The hydraulic press machine (a) and the Ti-Nb green compact (b).

3.4 Vacuum arc remelting

The Ti-Nb green compacts were arc melted in a button vacuum arc furnace to produce 100g ingots. A water-cooled copper hearth was used as a sample holder. A titanium ingot was used as an oxygen getter which was melted before the Ti-Nb samples to remove any impurities that may still be in the furnace. The furnace was purged with argon or helium and evacuated three times prior to each melting step. The samples were arc melted by using a non-consumable tungsten electrode. The heating and melting of the metal were achieved by the formation of the electric arc that was created between the tungsten electrode which acts as a cathode and the molten metal pool that formed on top of the ingot that acts as an anode. The ingot was cooled by a water-cooling system attached to the furnace. The samples were turned and remelted three times to ensure chemical homogeneity. Figure 3.3 shows the button vacuum arc furnace used for the remelting.

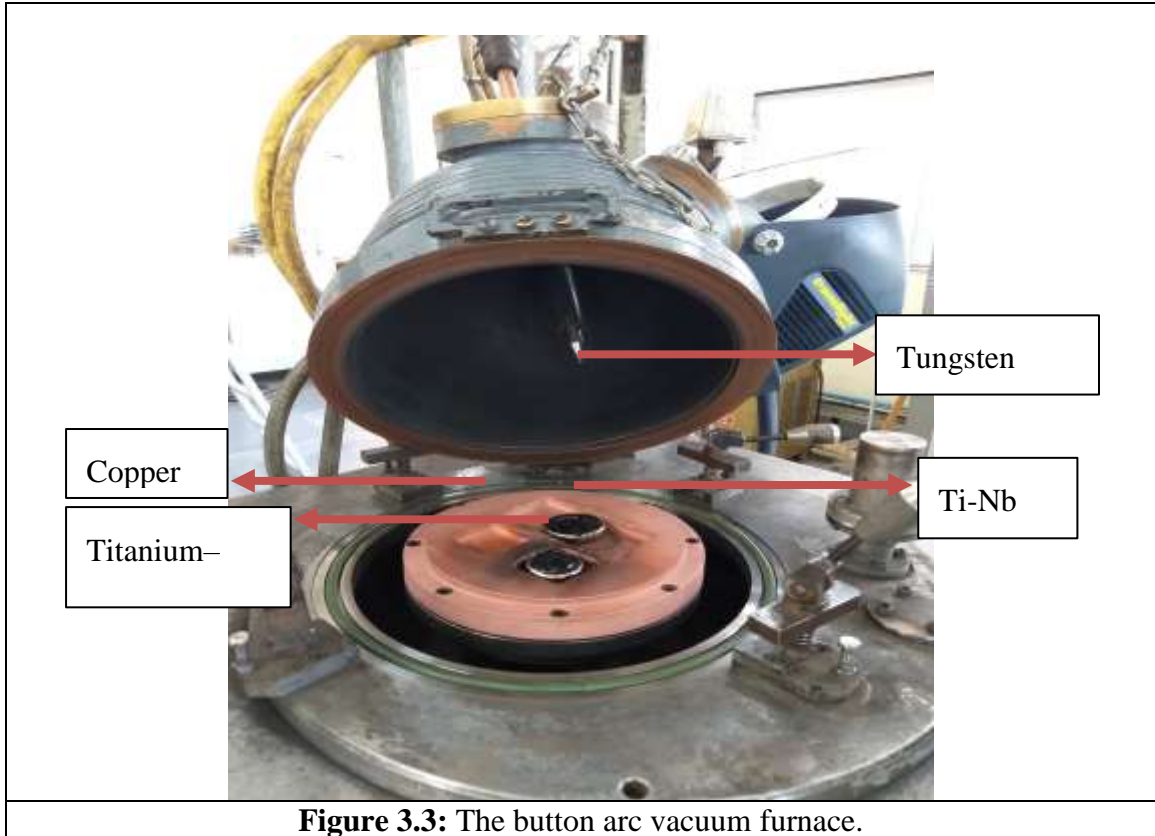


Figure 3.3: The button arc vacuum furnace.

3.5 Heat treatment

The as-cast samples were solution-treated using the Naber N150 muffle furnace. The samples were heated up to 1000 °C above the beta-transus temperature and held at this temperature for 3 hours. The samples were then cooled using furnace cooling, air cooling and water quenching. The furnace cooled samples were left in the furnace to cool overnight. The air-cooled samples were removed from the furnace at 1000 °C after the 3 hours to cool in air and the water quenched samples were removed from the furnace at 1000 °C immediately it reached the 3 hours and rapidly dropped in distilled water at room temperature.

3.6 Metallographic sample preparation

The as cast and solution-treated samples were precision sectioned/cut using the ATA Brilliant 221 cutting machine using a diamond cut-off wheel. The cutting speed was 4000 rpm with a feeding rate of 5mm/min. The cut specimens were hot mounted on the ATA OPAL 450 mounting machine using the Struers multifast black Bakelite hot mounting resin with wood filler thermosetting. The mounted samples were ground and polished using the ATA Saphir 550 automatic polishing machine. The samples were wet ground on Struers SiC papers with grit ranging from P800 to P2000 for 3 minutes on each paper. The samples were polished with a 3 μm diamond suspension for 3 minutes and colloidal silica for 6 minutes on a polishing pad/cloth to a mirror finished surface. The speed of 250-300 rpm was used for both grinding and polishing, with a force of 20N applied at the center of the sample to ensure consistent grinding and polishing of the sample. The polished samples were chemically etched using Kroll's etchant (2 ml HF, 6 ml NH_4OH , 92 ml distilled H_2O) for Ti- (1-13wt %) Nb compositions and (5 ml HF, 10 ml NH_4OH , 85 ml distilled H_2O) for Ti- (28-49wt %) Nb compositions ¹. The samples were immediately rinsed in water after etching to stop the corrosive action of the etchant followed by rinsing with ethanol and then blow dried.

3.7 Metallographic and phase characterization

The microstructural analysis of the as cast and solution-treated samples were analyzed using the Leica DMI5000M Optical Microscopy (OM) with the Image Pro Plus image analysis software. The samples were analyzed for phases and chemical composition/homogeneity using the Jeol JSM-6510 Scanning Electron Microscopy (SEM) equipped

with electron dispersive spectrometry (EDX). The secondary electron imaging and backscatter electron signals were used for the surface and phase analysis, the accelerating voltage used was 15 kV. X-ray diffraction (XRD) for phase analysis of the samples was done using the PANalytical X'Pert™ Pro powder diffractometer in θ - θ configuration with an X'Celerator™ detector with Fe filtered Co-K α radiation ($\lambda=1.789\text{\AA}$). The phases were identified using X'Pert Highscore Plus. The phase transformations of the as-cast samples were determined using the NETZCH STA 449F3. The simultaneous thermal analyser (STA) is a thermogravimetric analysis/differential scanning calorimetry (TGA/DSC) instrument used for thermal analysis. The STA output data from measurements is differential heat flow (DSC), sample mass change (TGA), and temperature as a function of time ³⁹. Differential scanning calorimetry technique was used for studying the phase transformations and reactions which involved heat absorption or heat release. The DSC measures the heat flow required to keep the sample and the reference at the same temperature ^{39,40}. A change in the heat flow corresponds to an endothermic or exothermic reaction which signifies phase transformations that were occurring in the sample. The measurements were carried out under argon flowing at 20ml/min to prevent sample oxidation. Prior to each measurement, the furnace was purged two times. The samples were heated up to 1200 °C at a heating rate of 10 °C/min and held for 30 minutes before cooling at the same rate to room temperature. The alumina crucibles were used for analysis with a corresponding alumina reference crucible. The transformation temperatures were extrapolated from the original graphs.

3.8 Mechanical testing

The micro-hardness of the as cast and solution-treated samples was measured using the Vickers micro-hardness tester. Each sample was indented with a 500 g force and dwelling time of 15 seconds. Ten hardness indentations were made and measured across each sample. The average, standard deviation and standard error were calculated for each of the samples.

The tensile specimens for tensile testing were prepared from the as-cast ingots through the electrical discharge machining. The dimension of the tensile specimens is illustrated in figure 3.4 below. The tensile samples are smaller than specified standard samples, the measured results might deviate from the standard sample size. Nevertheless, the small samples can still reflect the bulk mechanical properties if described by continuum medium mechanics. In addition, using data processing techniques such as conversion of elongation and inverse FEM the test results obtained from small samples can be converted to standard samples ⁴⁷.

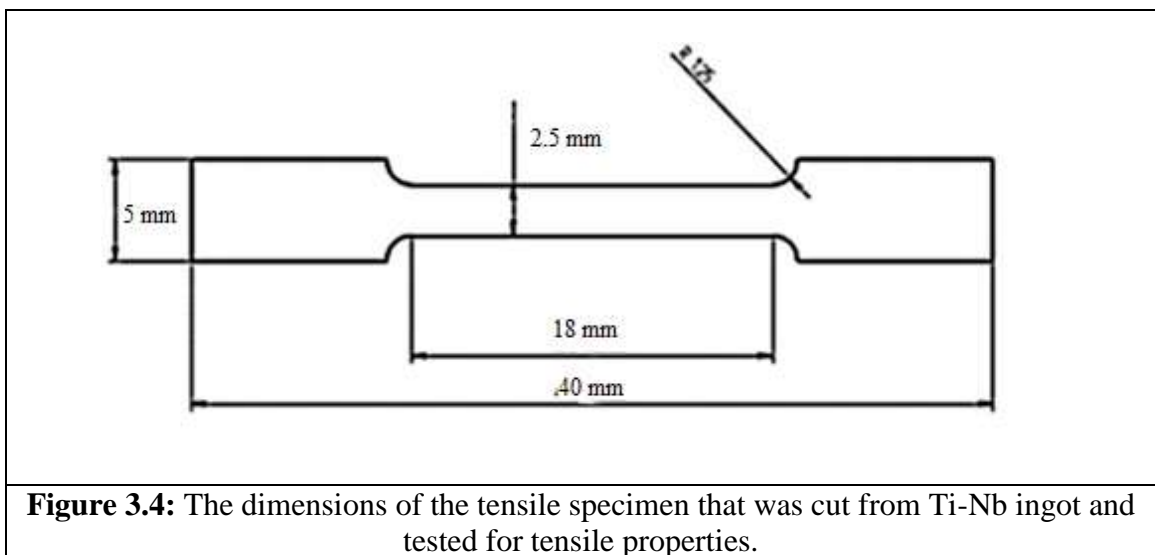
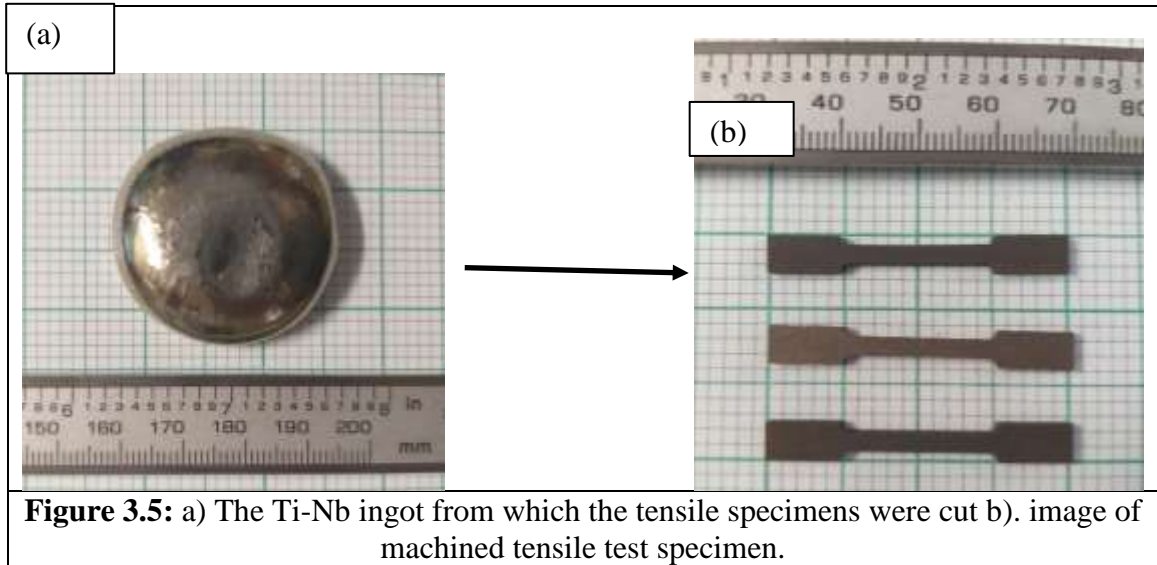


Figure 3.4: The dimensions of the tensile specimen that was cut from Ti-Nb ingot and tested for tensile properties.



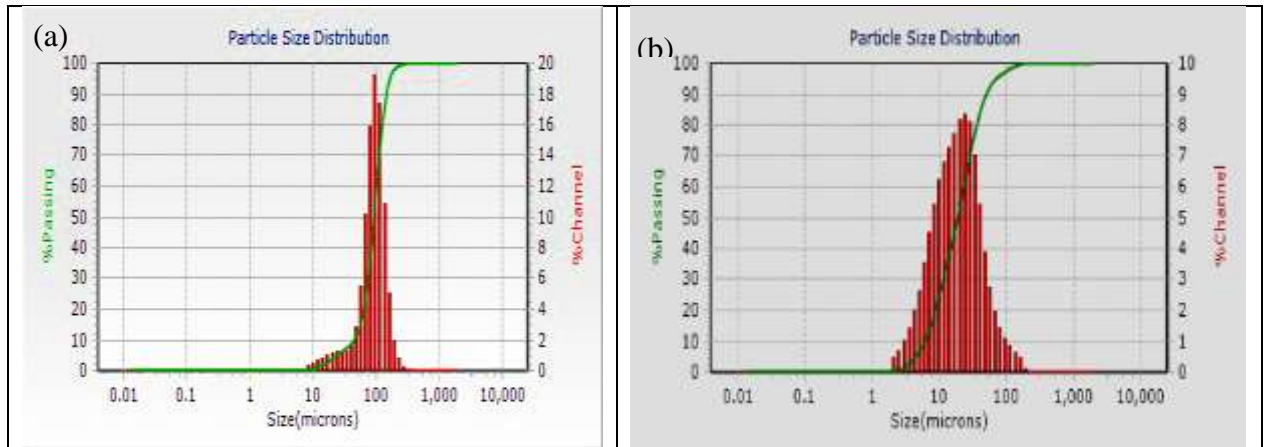
The as-cast Ti-Nb alloys tensile specimens were tested using the InstronTM 1342 tensile tester at room temperature. The strain was measured by using an extensometer attached to the gauge section of the specimen; the extensometer was then removed after an extension of about 1 mm to prevent its damage due to specimen fracture. The remainder of the strain was measured by the tensile tester until the specimen fractured. The ultimate tensile strength, 0.2 % yield strength, elongation and elastic modulus of the alloys were measured.

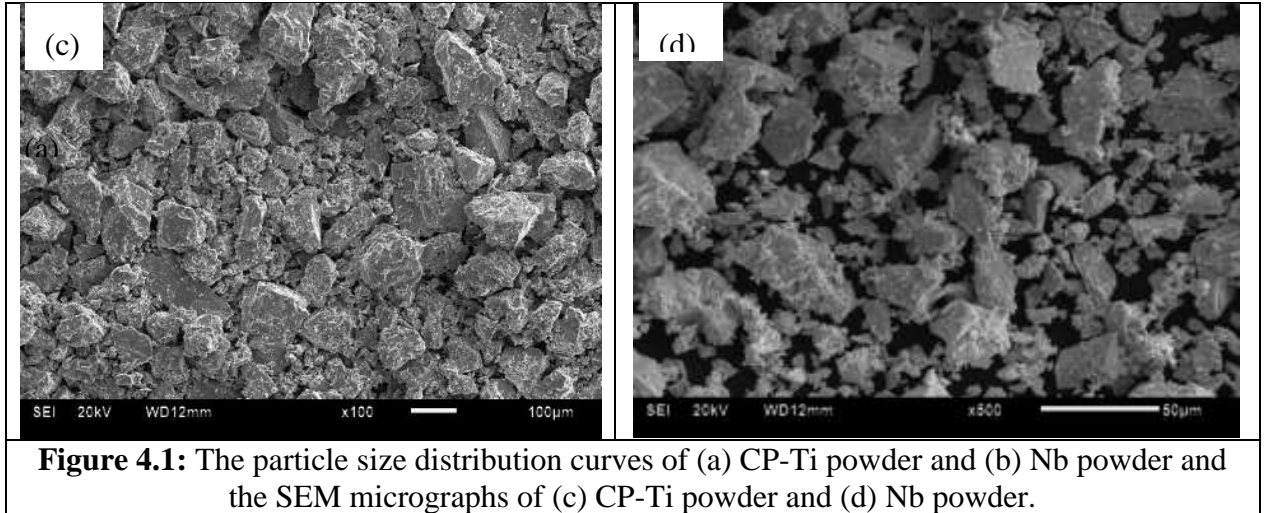
CHAPTER 4. RESULTS

This chapter presents all the results acquired from the tests carried out on the as-cast and solution treated Ti-Nb alloys. The results present the effect of Nb content on the microstructural evolution of the alloys obtained from the OM and SEM-EDX. The results of the phase analysis done using the XRD and the phase transformations of the alloy analysis using the simultaneous thermal analyser are also presented. The test results of the influence of the Nb content on the mechanical properties of the Ti-Nb alloys conducted using tensile test and micro-hardness measurements are presented.

4.1 Characterization of the starting powders

The particle size distribution curves and the SEM micrographs of the starting CP-Ti and Nb elemental powders are shown in Fig. 4.1.





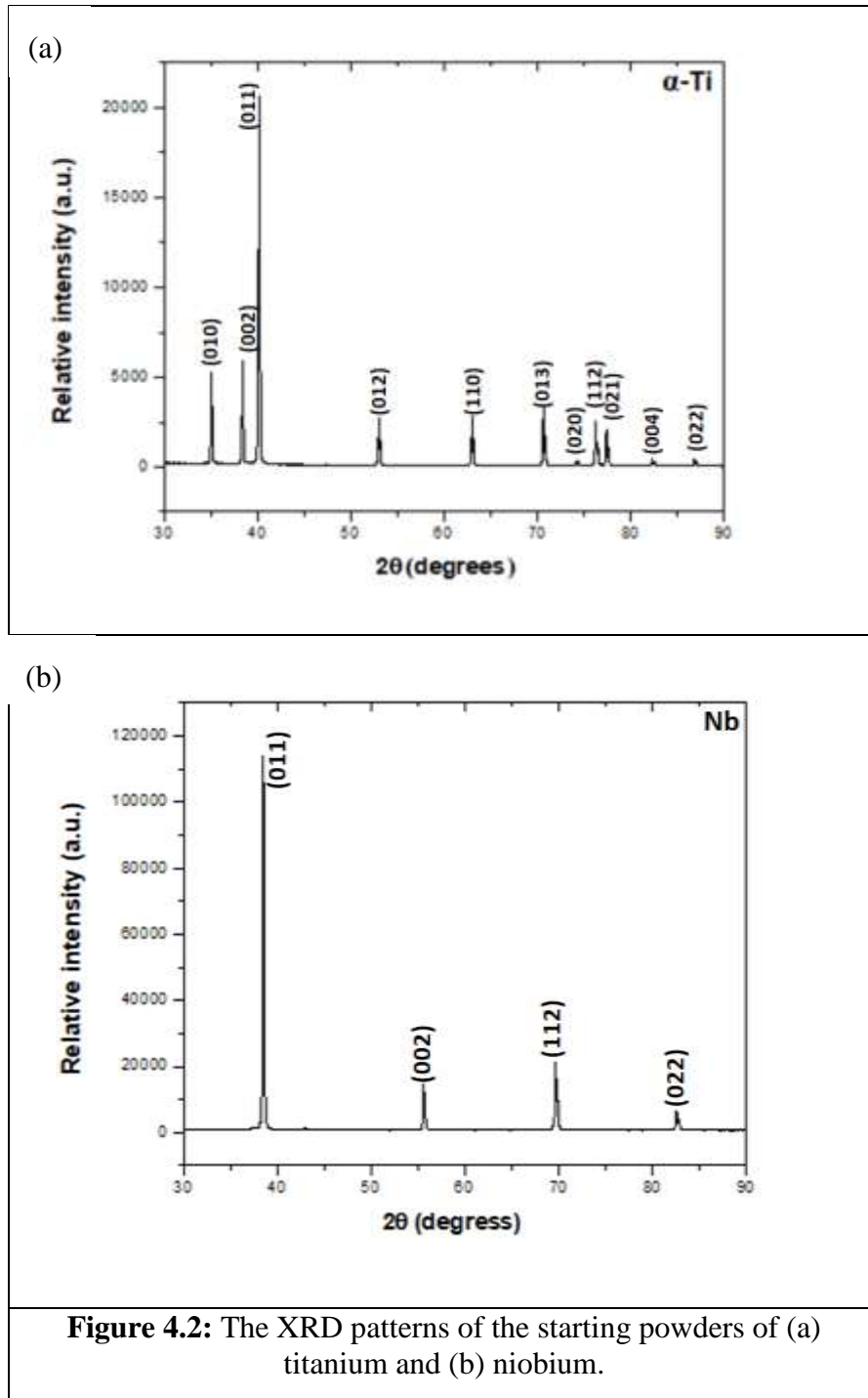
The particle size analysis shows that the d_{50} particle size is 92.71 μm and 18.61 μm for titanium and niobium, respectively; d_{10} and d_{90} particle sizes of the powders are given in Table 4.1. The particle distribution analysis of titanium shows that it contains coarse powder particles whereas niobium has fine particles as confirmed in the SEM micrographs as well. The titanium and niobium powders both consisted of block irregular shaped particles as shown in Fig. 4.1 (c) and (d). The oxygen content of the starting powders was measured using the gas fusion technique. The determined oxygen content of CP-Ti was 0.22 wt.% and 0.39 wt.% for Nb as shown in Table 4.1.

Table 4.1: Particle sizes of the starting powders and the particle size given by the supplier.

Powders	Measured particle sizes			Oxygen content
	$d_{10}(\mu\text{m})$	$d_{50}(\mu\text{m})$	$d_{90}(\mu\text{m})$	(wt.%)
CP-Ti	44.27	92.71	142.50	0.22
Nb	6.05	18.61	50.37	0.39

The XRD analysis of the starting elemental powders were done to identify the phases present in the powders. The XRD patterns of the starting elemental powders of CP-Ti and

Nb are shown in Fig 4.2. The CP-Ti showed that it has the hexagonal close packed crystal (HCP) structure which is an alpha (α -) phase. The XRD pattern for Nb showed that it has the body centred cubic crystal (BCC) structure.



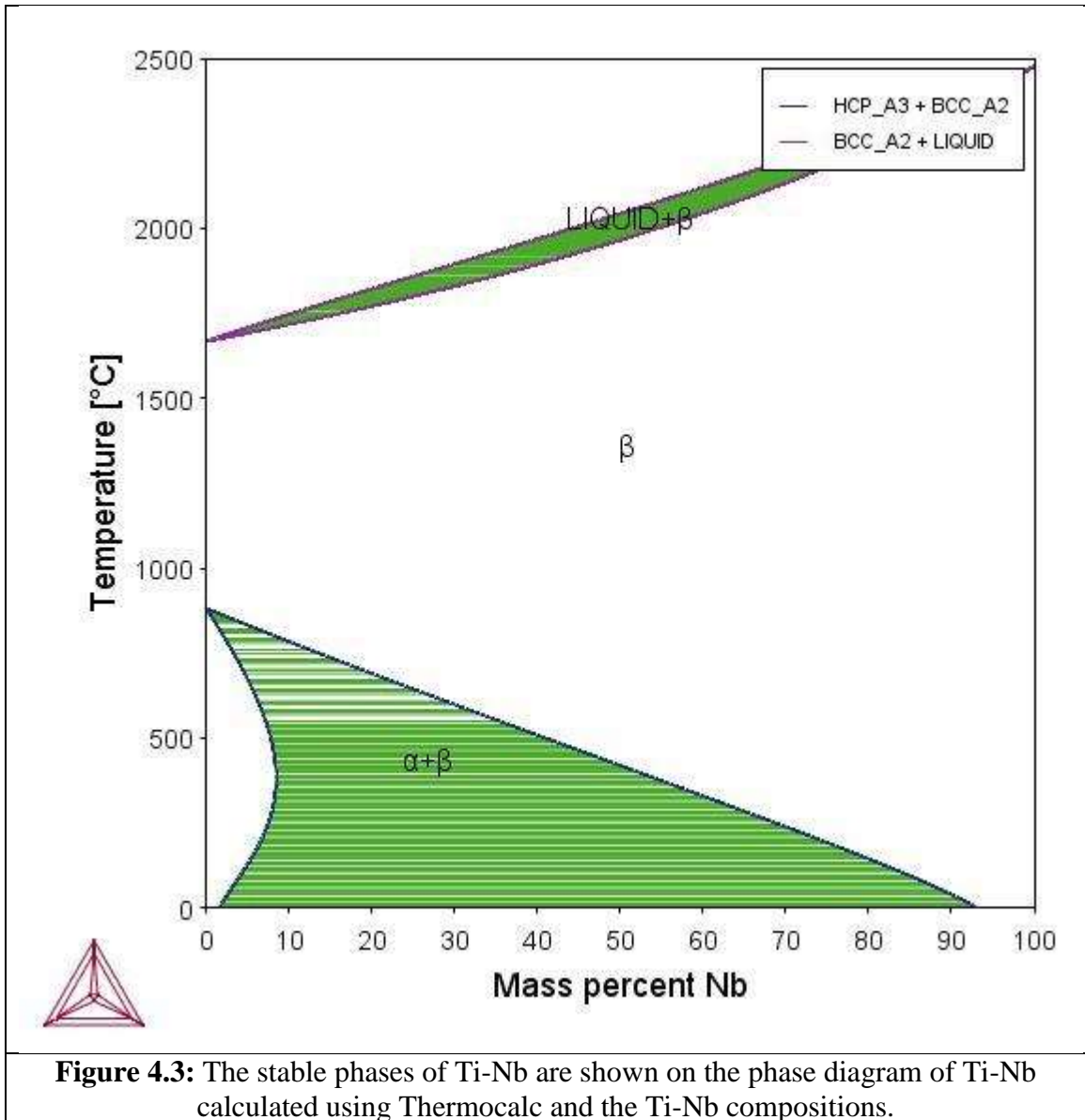


Figure 4.3: The stable phases of Ti-Nb are shown on the phase diagram of Ti-Nb calculated using Thermocalc and the Ti-Nb compositions.

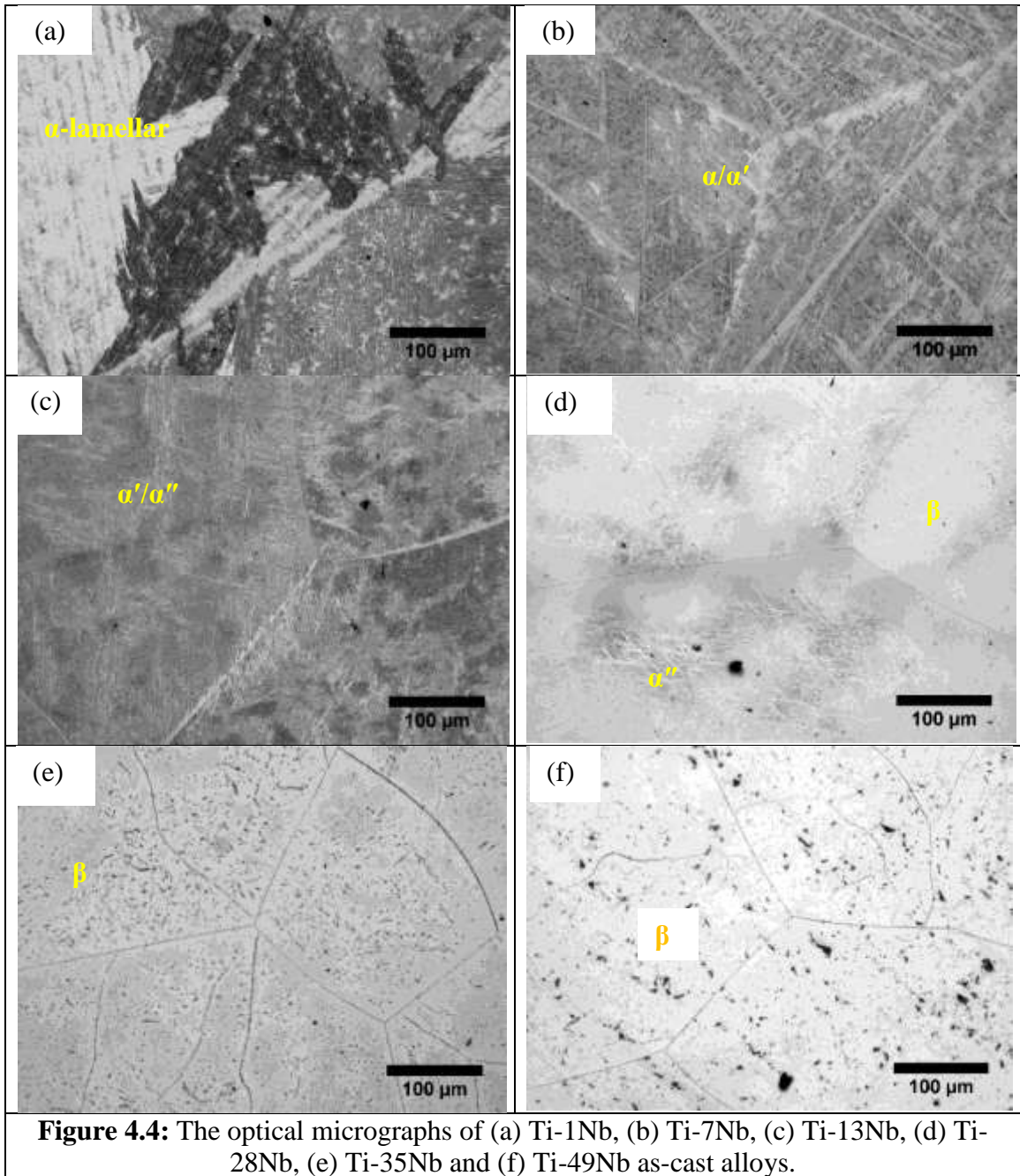
The phase diagram of Ti-Nb is illustrated in Fig 4.3 showing the stable phases of Ti-Nb as the Nb content increases from 0 to 100 wt.% over a temperature range of 0-2500 °C. The high temperature β -phase can be stabilized from as low Nb content as 2 wt.% as shown in the figure in phase composition with the α -phase. The transformation temperature from the β -phase to the α -phase decreases with increasing Nb content.

4.2 Characterization of the Ti-Nb alloys

The Ti-Nb alloys with the composition range of (1, 7, 13, 28, 35 and 49) were fabricated using the vacuum arc remelting process to investigate the effect of Nb content on the as-cast and solution-treated alloys. The microstructural and phase analysis of the alloys was done to determine their evolution as the Nb content increased. The tensile properties of the Ti-Nb alloys were determined to study the effect of Nb content on the mechanical properties of the alloys.

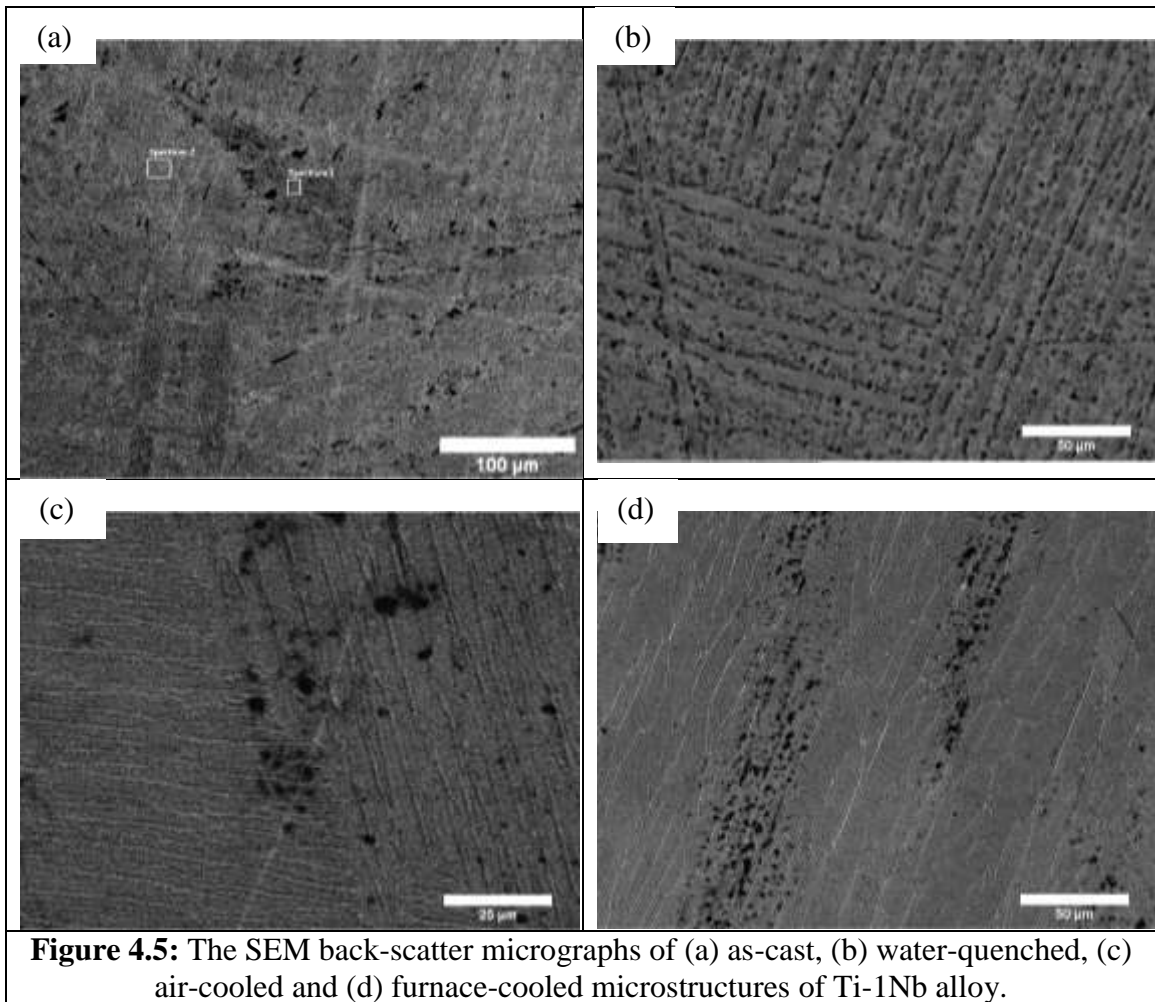
4.2.1 *Microstructural analysis of the as-cast and solution-treated Ti-Nb alloys*

The optical micrographs that illustrate the microstructural evolution of the as-cast Ti- (1-49) Nb alloys are shown in Figure 4.4. Alloying CP-Ti with 1 wt.% Nb resulted in α -lamellar microstructures as shown in Fig. 4.4(a). The lath-type α/α' -martensitic microstructure was observed for the Ti-7Nb alloy. As the Nb content was increased to 13wt.%, the microstructure observed was the acicular martensite. Acicular α' -martensite and α'' -martensite are morphologically similar; however, they can be distinguished with phase analysis by XRD as they have different crystal structures. The martensitic structure evolved from the lath-type to the fine acicular microstructure as the Nb content increased from 7wt% to 13wt% as seen in the optical micrographs in Fig 4.4 (b & c). In Ti-28Nb alloy, a mixture of fine acicular α'' -martensitic microstructure and the metastable β -phase were observed. Ti-35Nb and Ti-49Nb alloys both exhibited equiaxed β -phase with sub-grain boundaries inside.



Heat treatment of the Ti-alloys is a way to design microstructures and different phases, as the phases obtained directly influence the mechanical properties of the alloys. The microstructural evolution of the Ti-Nb alloys solution treated at 1000 °C/3h and cooled in the furnace, air and water to room temperature is illustrated in Figure 4.5 to 4.11. The SEM micrographs of Ti-1Nb shown in Fig. 4.5(a-d), exhibiting the obtained microstructures of

the as-cast, water-quenched, air- and furnace-cooled samples. The microstructures of the as-cast and the solution treated samples of Ti-1Nb alloys exhibited the α -lamellar microstructure. The width of the α -lamellar structures differed for the as-cast and solution-treated samples as well the size of the α -lamellar colonies. The width of the α -lamellar structures decreased as the cooling rate increased from the furnace-cooled to the air-cooled sample, which had the smallest width.



The microstructures of Ti-7Nb alloy evolved from α/α' -laths for the as-cast sample to acicular α' -martensite for the water-quenched sample and to α -lamellar colonies for the air- and furnace cooled samples, was shown in Fig. 4.6. The α -lamellar microstructure had the

β -phase retained between the α -lamellar structures for the furnace-cooled sample as seen in the micrograph in Fig. 4.6(d). The width and the colony size decreased as the cooling rate increased from furnace cooling to air cooling. As the cooling rate increased for the water-quenched sample, the microstructure fully transformed into a homogeneous acicular α' -martensite.

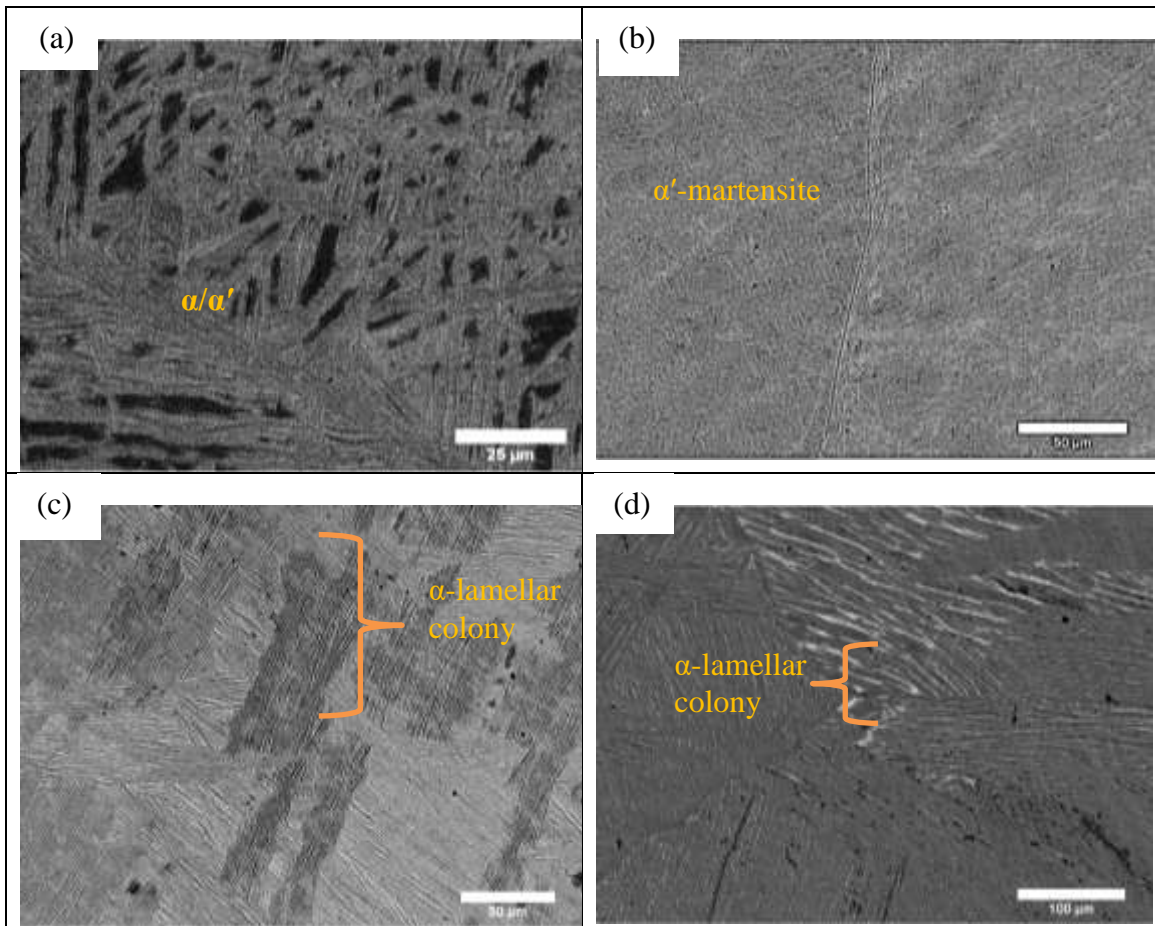
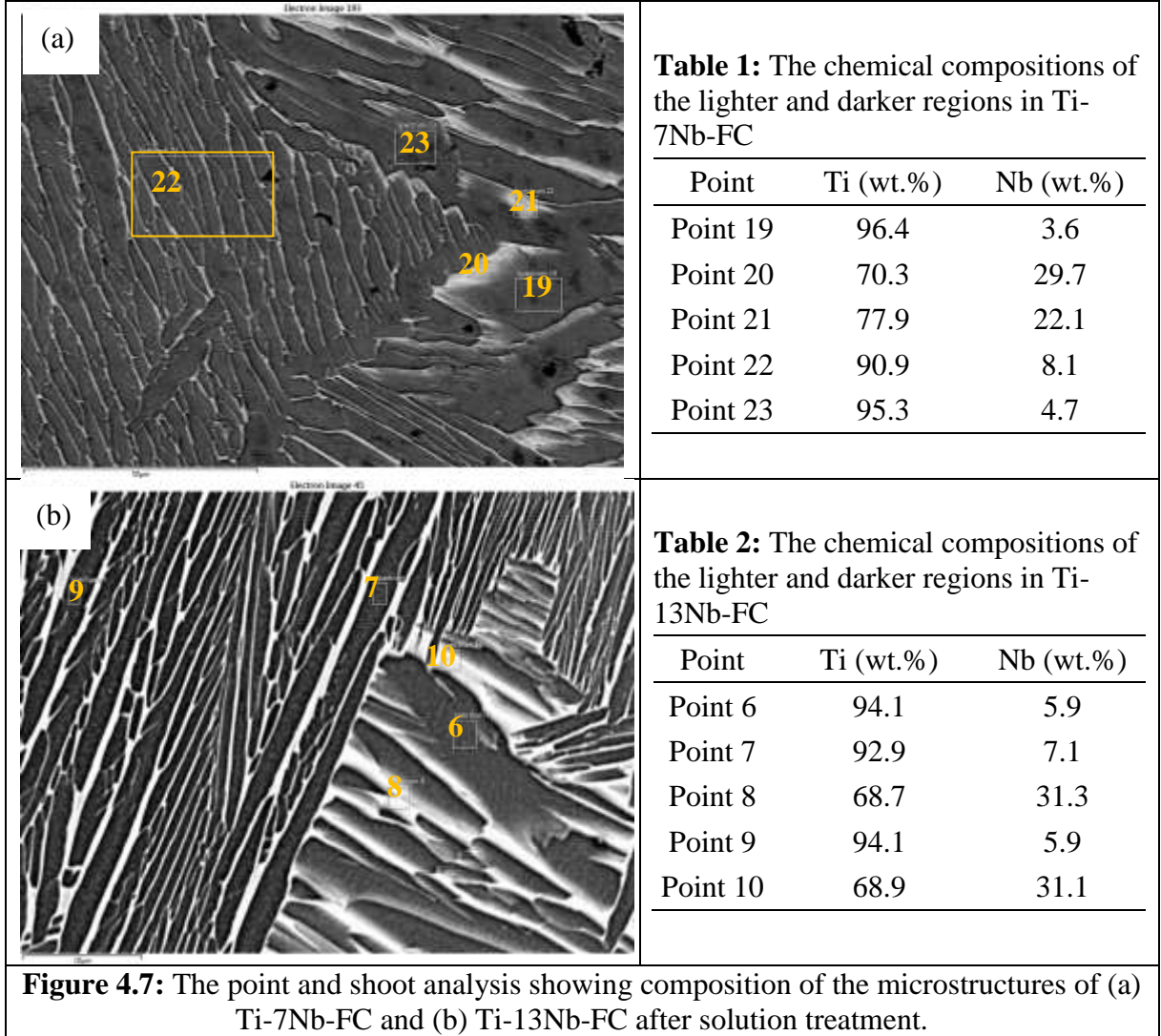


Figure 4.6: The SEM back-scatter micrographs of (a) as-cast, (b) water-quenched, (c) air-cooled and (d) furnace-cooled microstructures of Ti-7Nb alloy.

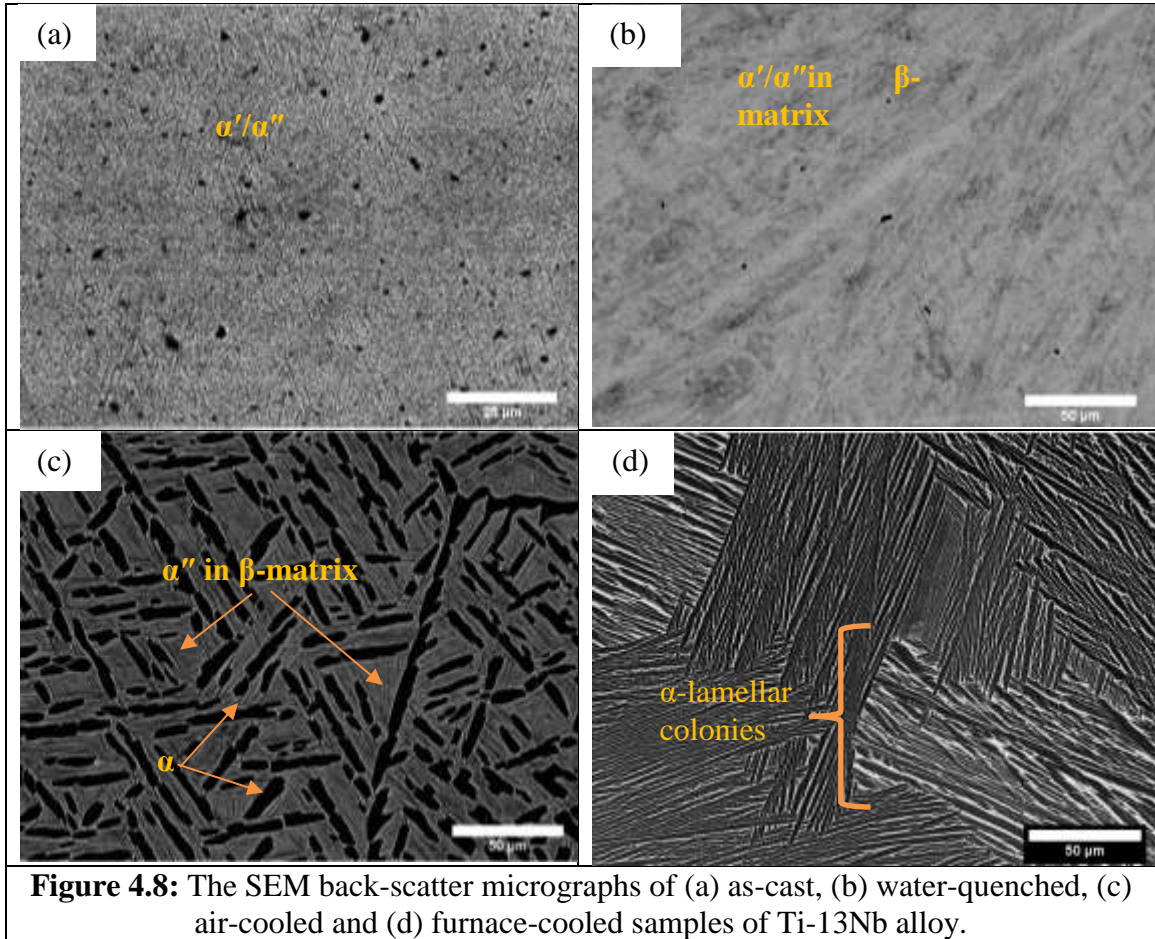
The compositions of the furnace-cooled Ti-7Nb and Ti-13Nb alloys which were done using SEM-EDX point and shoot analysis are shown in Fig. 4.7 and Table 1 and 2. The lighter regions in the α -lamellar microstructures were analysed to be Nb-rich as shown by the high

Nb-content and the darker regions found to be Ti-rich. The Nb-rich regions were found to retain β -phase in the lamellar microstructure as Nb is a β -stabilizing element.

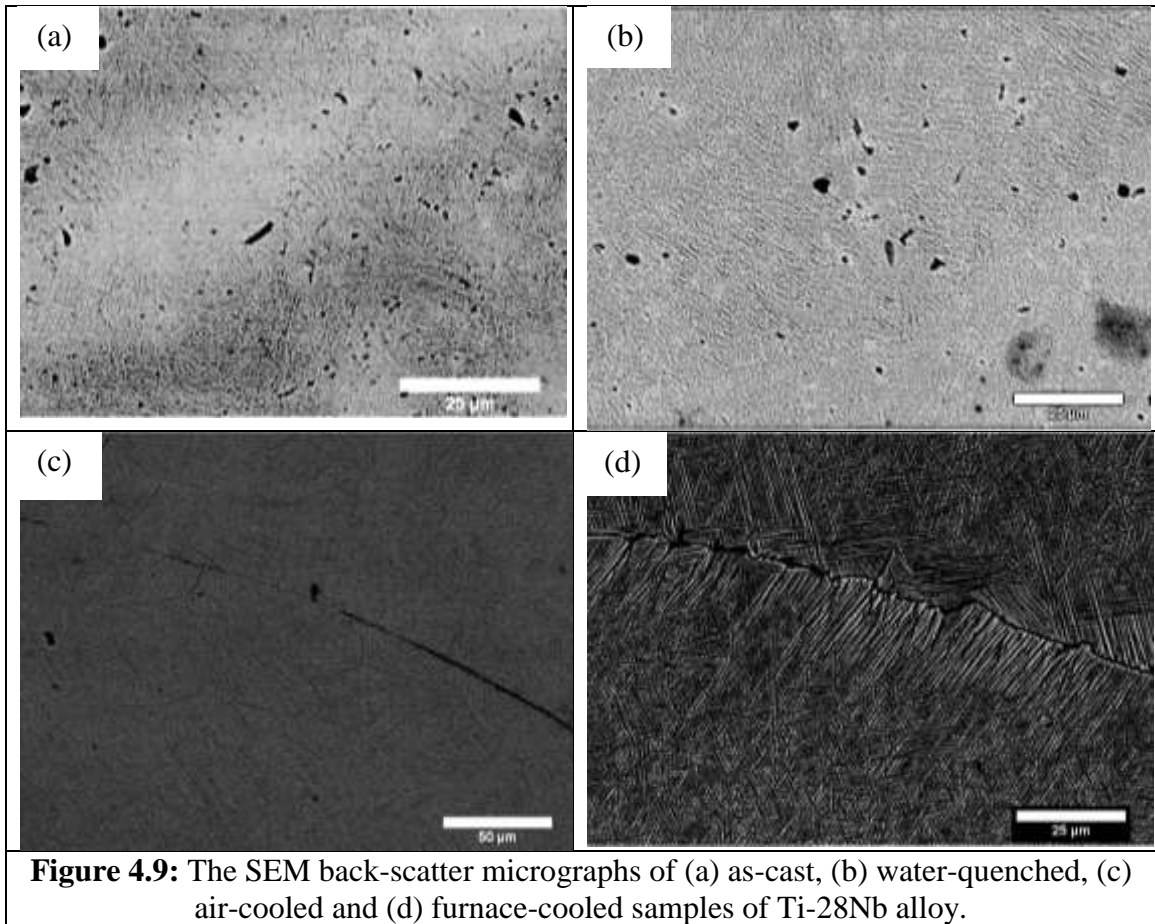


The microstructures of Ti-13Nb alloy for the as-cast and solution treated samples are shown in Fig. 4.8. The α'/α'' -martensitic microstructure of the as-cast Ti-13Nb nucleated into different combinations of α , α' , α'' and β microstructures as the alloy was cooled using different cooling mediums from the β -field after solution treatment. The Ti-13Nb alloy exhibited α/β -lamellar colonies for the furnace-cooled sample as shown in Fig. 4.7(b). As the cooling rate increased; the α'' -martensite nucleated within the β -phase matrix with

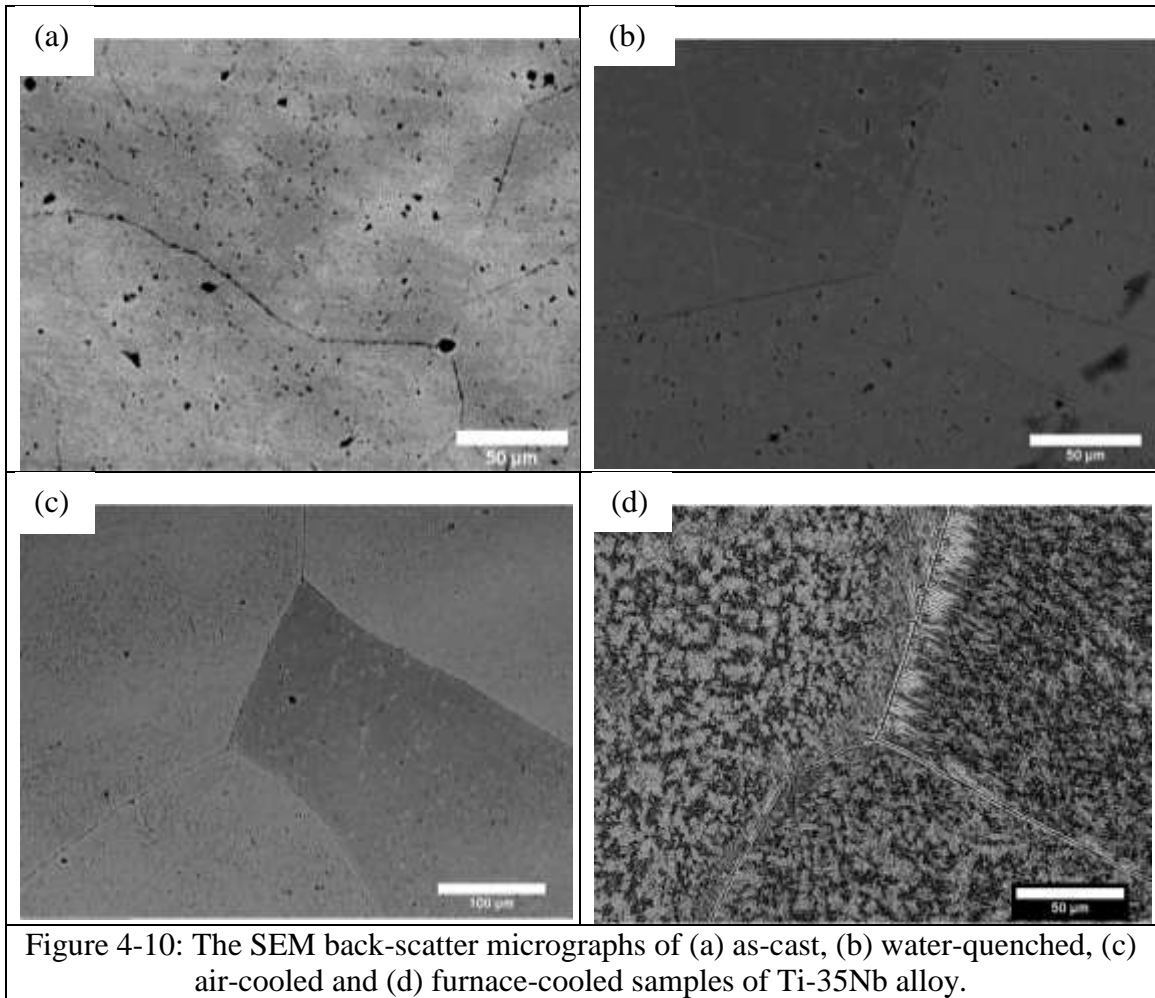
globular α -phase grains for the air-cooled sample. At the fast-cooling rate in the water-quenched sample, the microstructure evolved to fine acicular martensite within the β -phase matrix.



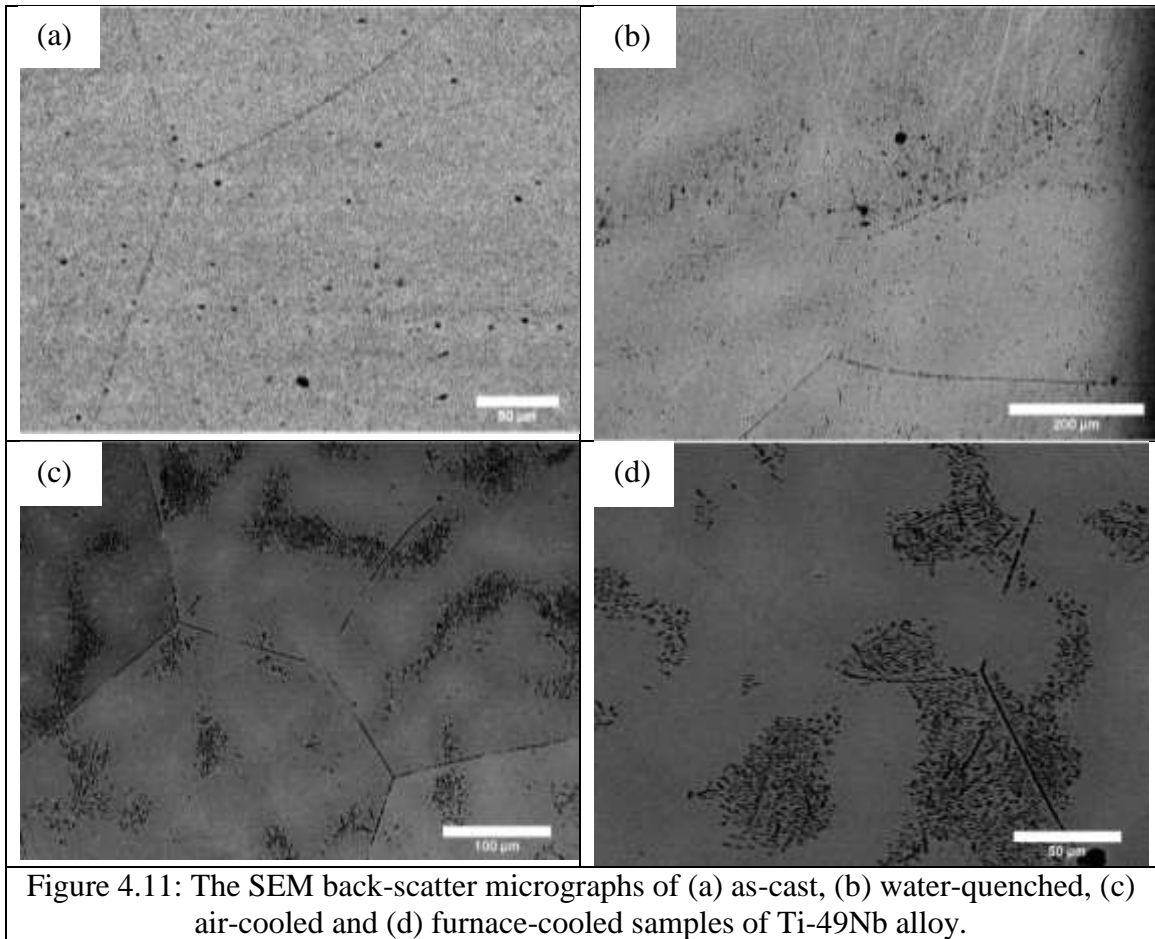
The microstructures obtained for the as-cast and the solution-treated samples for Ti-28Nb alloy are shown in Fig. 4.9. The as-cast sample had an α'' -martensitic and β -phase structure. The needle-like martensitic microstructure nucleated from the β -grain boundaries and within the grain as the sample was furnace-cooled from the β -phase field. As the cooling rate was increased for the air-cooled sample, fine acicular α'' -martensitic microstructure transformed with inter-granular α -grains. When the sample was fast cooled, a metastable β -phase was obtained with finer α'' -martensitic microstructures within the β -matrix.



The microstructural evolution of the solution-treated samples that were cooled at different cooling mediums and the as-cast sample for Ti-35Nb alloy are shown below in Fig. 4.10. Acicular martensitic microstructures precipitated from the β -grains and within the β -phase matrix for the furnace-cooled sample. A metastable β -phase was retained with very refined α'' -martensitic microstructures that transformed inside the β -grains as the cooling rate increased for the air-cooled sample. The as-cast and water-quenched samples both had fully retained β -phase as shown in Fig. 4.10(a & b). The furnace- and air-cooled samples had martensitic microstructures indicating that the amount of Nb was not enough to suppress their formation when the sample was slow cooled from the β -phase field.



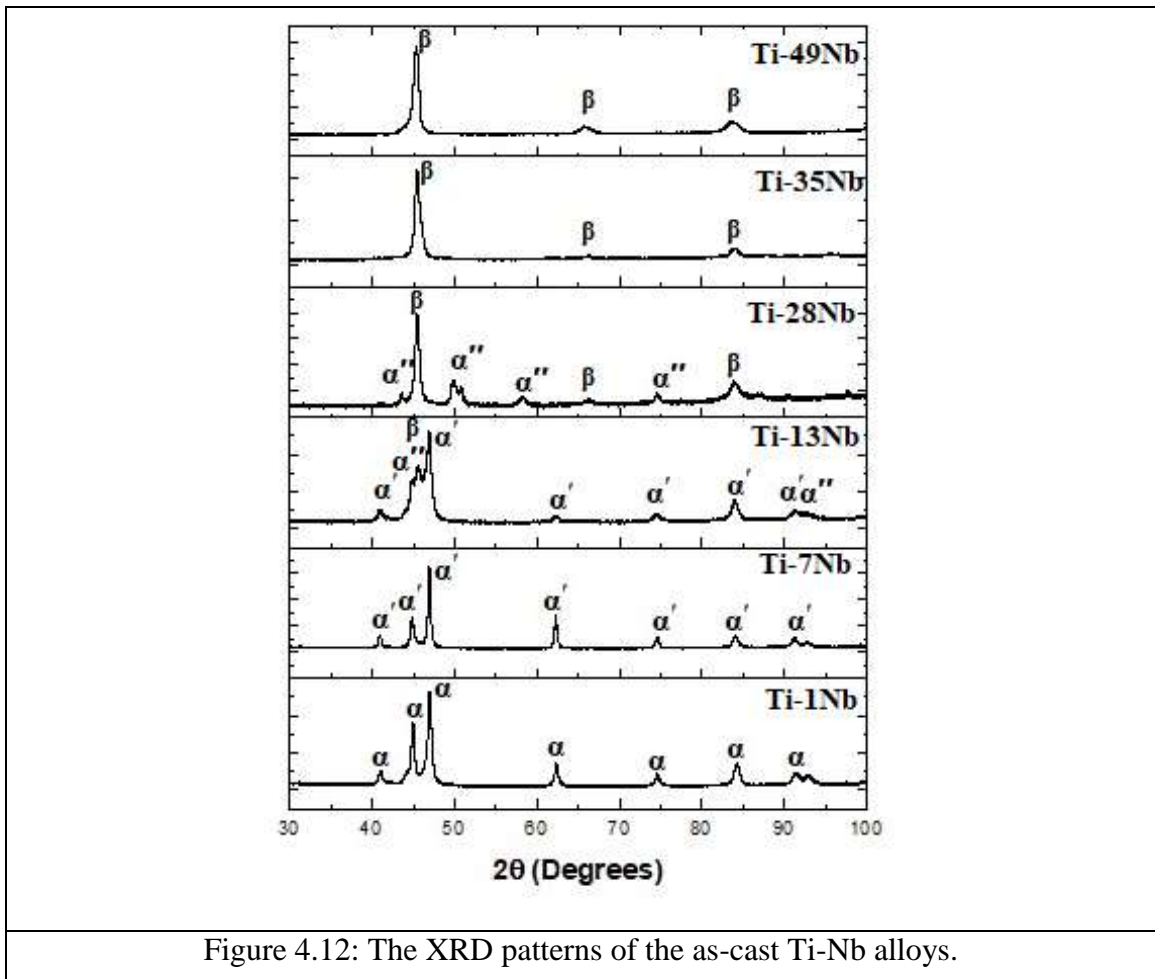
The microstructures of the as-cast, water-quenched, air- and furnace-cooled samples of the Ti-49Nb alloy are shown in Fig. 4.11. The β -phase was fully retained for the as-cast sample. As the sample was slowly cooled as in the furnace- and air-cooled processes, the β -phase was retained with anomalous structures within the β -phase and along the grain boundaries. The Ti-49Nb alloy is expected to fully retain the β -phase due to the high Nb content. As the sample was fast cooled, the β -phase was fully retained as shown in Fig. 4.11(b).



4.2.2 Phase analysis of the as-cast and solution-treated Ti-Nb alloys

The phases obtained in the Ti-Nb alloys after the vacuum arc remelting process and solution treatment were identified using the XRD. The XRD patterns of the as-cast Ti-Nb alloys are shown in Fig. 4.12. The phase retained for Ti-1Nb alloy is the α -phase as exhibited by the hexagonal close packed crystal structure pattern. Therefore, the Nb amount added to CP-Ti was not enough to induce change in the crystal lattice structure of CP-Ti. The crystal structure obtained for Ti-7Nb showed an hexagonal close packed crystal structure. The α -phase and α' -martensitic phase both have the hexagonal closed packed structure, however, these phases can be distinguished by their microstructures. The main phase found by XRD analysis for Ti-13Nb alloy is the α' -hexagonal crystal structure and

some α'' -orthorhombic crystal structure and the β -phase, body centred cubic crystal structure peaks were also detected. However, the β -phase was not identified by microstructural analysis for the Ti-13Nb alloy. When the content of Nb was increased to 28 wt.%, the presence of the body centred cubic crystal structure was identify as well as the α'' -orthorhombic crystal structure. The high temperature bcc β -phase was fully obtained for Ti-35Nb and Ti-49Nb alloys as shown in the XRD patterns of the alloys in Fig 4.11.



The XRD patterns of the as-cast Ti-Nb alloys and of the heat-treated samples that were cooled in the furnace, air and water are illustrated in Fig. 4.13-15 to show the evolution of phases transformed. The XRD patterns of the alloys exhibited different phase evolutions

as the cooling rate increased due to the different cooling mediums used after solution treatment as the Nb increased from Ti-1Nb to Ti-49Nb.

The α -hexagonal (HCP) crystal structure was obtained for the as-cast and solution-treated Ti-1Nb alloys as seen in Fig. 4.13. The change in cooling rate due to the cooling mediums did not lead to transformation of new phases in the Ti-1Nb alloy as it increased after solution treatment. Therefore, the Ti-1Nb content was not enough to induce transformation of the martensitic phases or the β -phase even after heat-treatment and applying different cooling rates. However, the different cooling rates did have an influence in the colony sizes and the width of the α -lamellar microstructures as seen in the SEM micrographs of Ti-1Nb in Fig. 4.5.

The distorted α' -hexagonal crystal structure was obtained for the as-cast Ti-7Nb alloy. The hexagonal crystal structure was obtained for the furnace- and air-cooled samples, however, for the furnace-cooled sample a small amount of the β -phase was as exhibited by the cubic (bcc) crystal structure peak as shown in Fig. 4.13. The β -phase peak in the furnace-cooled sample of Ti-7Nb is due to the retained β -phase in between the α -lamellar microstructures as shown in the SEM micrograph in Fig. 4.6(d). Even though the slow-cooled samples both had retained the α -phase, the α -lamellar microstructures differed in width and in colony size as shown in Fig. 4.6(c-d). Fast cooling of Ti-7Nb alloy after solution treatment in the β -phase field resulted in the distorted α' -hexagonal (HCP) crystal structure.

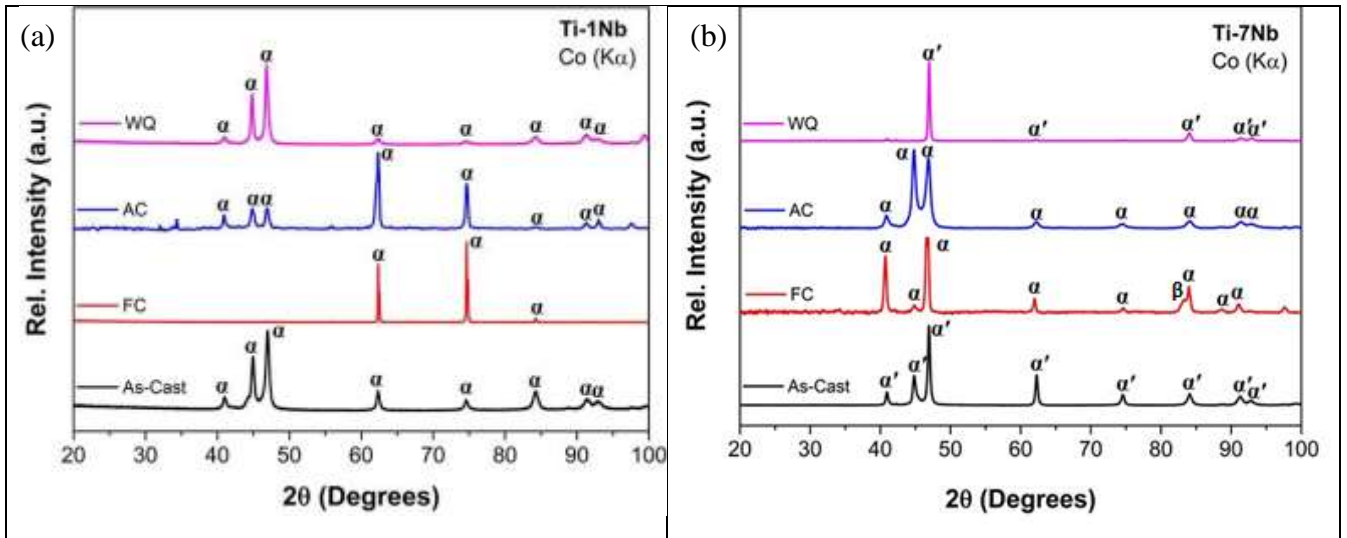


Figure 4.13: The XRD patterns of the as-cast, furnace-cooled (FC), air-cooled (AC) and water-quenched (WQ) samples Ti-1Nb and Ti-7Nb alloys.

The increase in Nb content to 13wt.% led to a mixture of equilibrium and non-equilibrium phases being retained after solution treatment. The hexagonal α -phase and a small amount of the cubic β -phase were obtained for the furnace-cooled sample of Ti-13Nb alloy. As the cooling rate increased for the air-cooled sample the orthorhombic α'' -martensite phase, α - and β -phase were retained as shown in the XRD pattern on Fig. 4.14. The fast-cooled sample showed a mixture of the hexagonal α' -martensite, orthorhombic α'' -martensite, and the β -phase. The acicular α' - and α'' -martensite are morphologically similar but were distinguished through XRD analysis. The α' - and α'' -martensite and β -phase were retained in the furnace-cooled Ti-28Nb samples. As the cooling rate increased for the air-cooled sample, a fully orthorhombic α'' -martensite phase was obtained as shown by the XRD pattern in Fig. 4.14. The increase in cooling rate as well as the increase in Nb content resulted in the fully α'' -martensitic phase. The meta-stable β -phase was retained in the water-quenched Ti-28Nb alloy with a small peak of the orthorhombic α'' -phase.

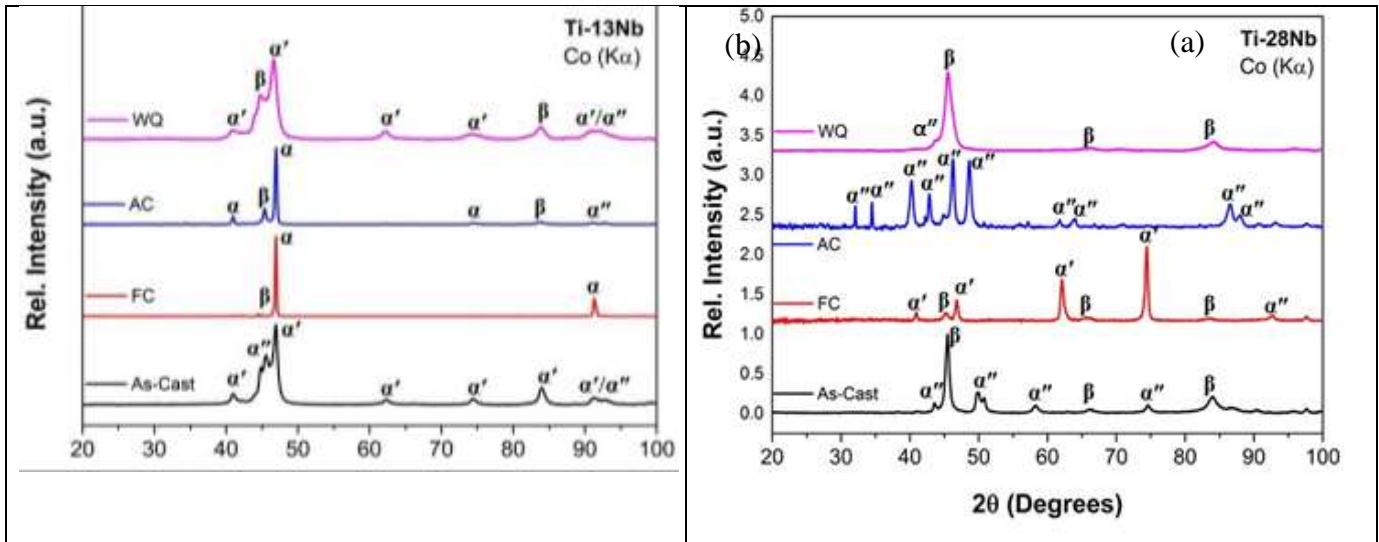


Figure 4.14: The XRD patterns of the as-cast, furnace-cooled (FC), air-cooled (AC) and water-quenched (WQ) samples Ti-13Nb and Ti-28Nb alloys.

The XRD patterns for Ti-35Nb and Ti-49Nb alloys are shown in Fig. 4.15 exhibiting the phases obtained for the as-cast and solution-treated samples. The metastable β -phase was obtained for the as-cast Ti-35Nb alloy. The furnace-cooled Ti-35Nb alloy after solution treatment had a mixture of α' - and α'' -martensite and the β -phase. The cubic β -phase was retained for the air-cooled sample with small peaks for the orthorhombic α'' -phase. The nucleation of the martensitic phases as the samples were slow cooled shows that the amount of the Nb content was not high enough to lower the M_s temperature below room temperature as the sample had enough time to nucleate the martensitic phases. Therefore, the fast cooling of the as-cast sample due to the water-cooled copper mold used for casting compared to the furnace-cooled sample led to the metastable β -phase being retained. When the cooling rate was increased for the water-quenched sample the cubic β -phase was fully retained.

The different cooling rates imposed by the different cooling mediums used after heat treatment of Ti-49Nb alloy did not have an influence on the cubic β -phase crystal structure

of the as-cast alloy as shown by the XRD patterns in Fig. 4.15. However, the SEM micrographs of the furnace- and air-cooled samples of Ti-49Nb alloy did show anomalous structures in the microstructure as shown in Fig. 4.10. Therefore, XRD analysis was unable to determine the nature of the structures in the furnace- and air-cooled samples of Ti-Nb alloy even though it picked up the β -phase.

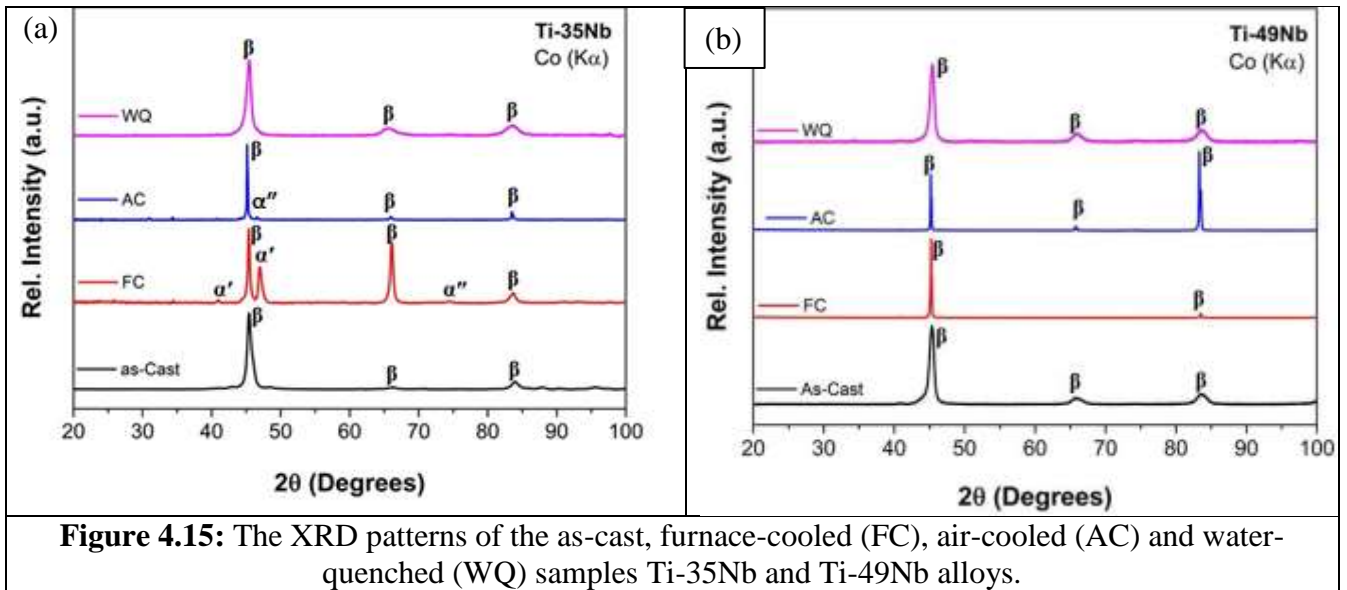


Figure 4.15: The XRD patterns of the as-cast, furnace-cooled (FC), air-cooled (AC) and water-quenched (WQ) samples Ti-35Nb and Ti-49Nb alloys.

4.2.3 Phase transformations of the as-cast Ti-Nb alloys

The thermal analysis of the as-cast Ti-Nb alloys was done using the differential scanning calorimetry (DSC) to determine the phase transformations that occurred in the alloys when heat is applied. The DSC curves of the Ti-Nb alloys are presented in Figure 4.16, showing endothermic and exothermic peaks which indicate the different phase transformations that occurred as the temperature was increased from room temperature to 1200 °C above the β -transus temperature.

In the as-cast CP-Ti, only one peak was detected indicating an endothermic reaction⁴¹. This endothermic reaction is due to the transformation of the α -phase into the β -phase. The

endothermic peak is approximately 920 °C, which is above the β -transus temperature of pure Ti which is approximately 882 °C. The Ti-1Nb and Ti-7Nb alloys also exhibited the α -phase to β -phase transformation endothermic peak as shown in Fig. 4.16(a). The addition of Nb to Ti caused the endothermic peak to shift to lower temperatures compared to the CP-Ti endothermic peak for Ti-1Nb and it continued to shift as the Nb content increased for the Ti-Nb alloys. In Ti-13Nb, the endothermic α to β transformation peak was observed, with additional peaks identified as seen in the zoomed in plot in Figure 4.16(b). The additional peaks show the transformation of the β -phase into ω -phase before it transforms to β . The transformation of the martensitic phases was not observed as expected as the alloy primarily consists of the martensitic phases.

As the Nb content increased to 28 and 35 wt.%, the phase transformation evolution changed as the heat increased with additional exothermic and endothermic reactions occurring. The first exothermic reaction has been identified as the β -phase transforming into isothermal ω -phase for Ti-28Nb and Ti-35Nb alloy. The phase transformations were expected as Ti-28Nb alloy had an initial phase composition of α'' -martensite and β -phase and Ti-35Nb alloy had the β -phase.. The formation of the ω_{iso} -phase is quickly followed by its transformation into the β -phase for both Ti-28Nb and Ti-35Nb alloys. The unstable β -phase decomposed into the α -phase, which in turn transformed to the β -phase as the temperature increased. For the single-phased Ti-49Nb alloy, no reactions were identified as the sample was heated, the high Nb content suppressed any kind of phase transformation, stabilizing the β -phase at any temperature.

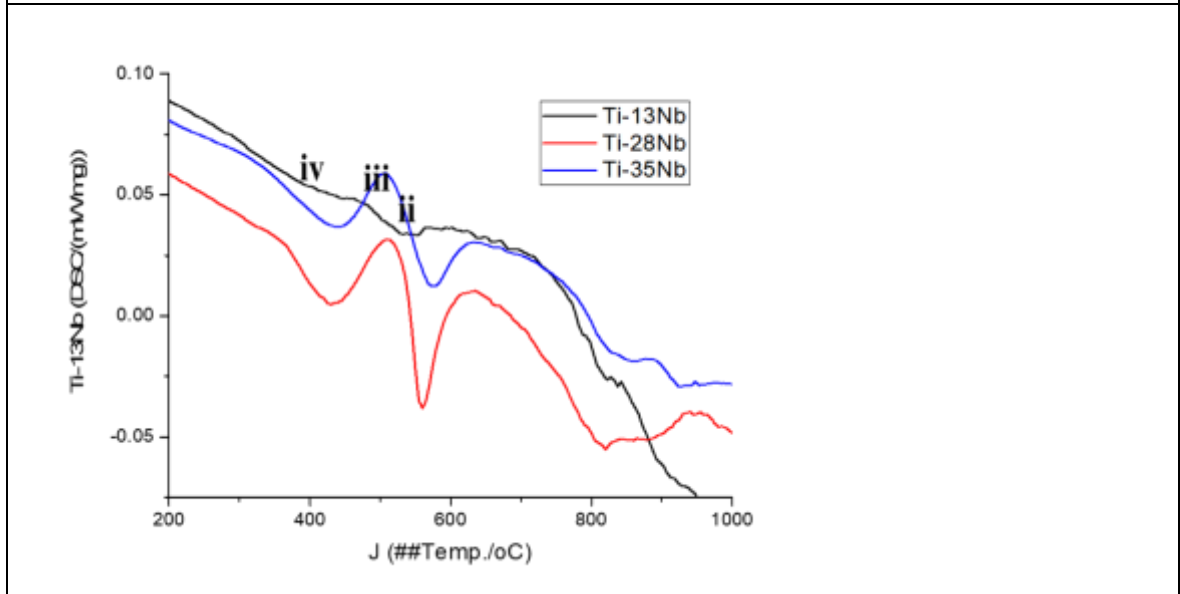
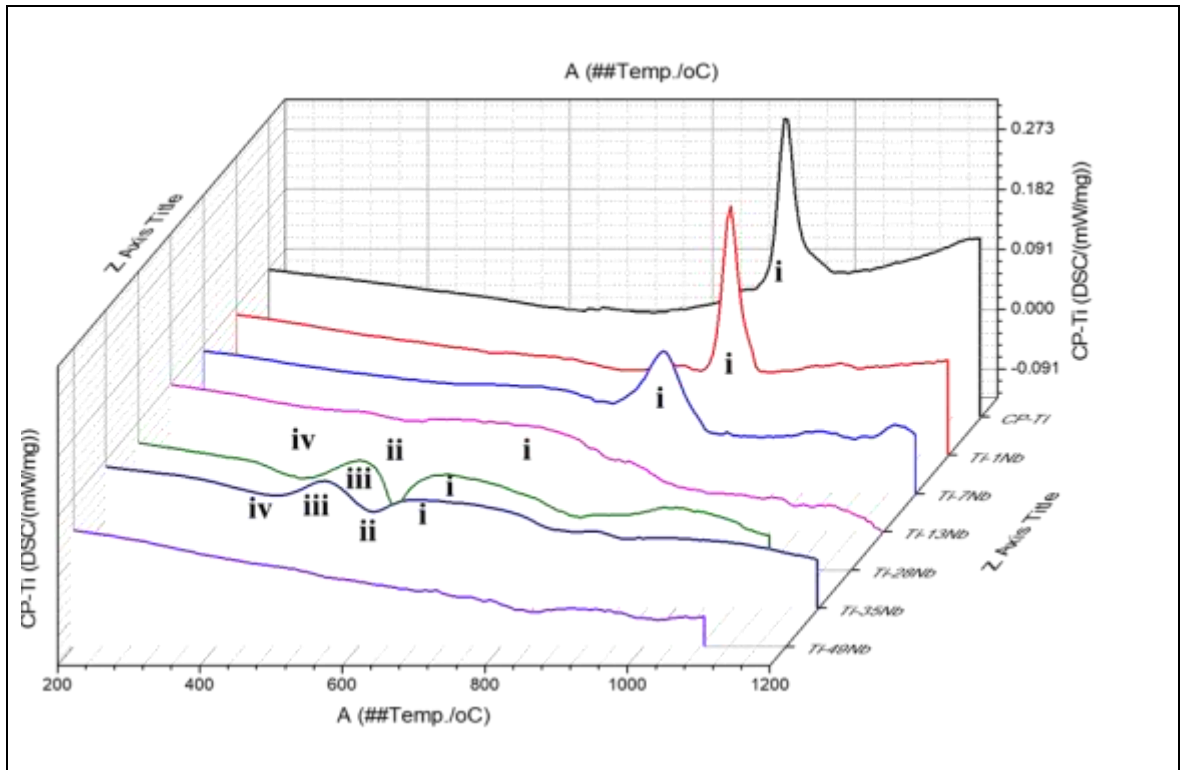


Figure 4.16: The DSC scans of the as-cast Ti-Nb alloys illustrating the endothermic and exothermic reactions as the alloys were heated from room temperature up to 1200 °C, (a) DSC curves for the Ti-Nb alloys and (b) DSC curves for Ti-13Nb, Ti-28Nb and Ti-35Nb alloy.

Table 4.2: The phase transformations of the endothermic and exothermic peaks in the DSC graph in Fig. 4.7 of the Ti-Nb alloys.

Peaks	Phase transformations
i	$\alpha \rightarrow \beta$
ii	$\beta \rightarrow \alpha$
iii	$\omega \rightarrow \beta$
iv	$\beta \rightarrow \omega$

The microstructural evolution of the Ti-Nb alloys as the Nb content increased and the phase transformations of the as-cast Ti-Nb alloys are illustrated in Table 4.3. The microstructures and phases observed in the alloys evolved from the α -phase in the CP-Ti and Ti-1Nb to martensitic phases as the Nb content increased to 7 and 13 wt.%. The metastable β -phase was retained for Ti-28Nb with the α'' -martensitic phase and then the β -phase fully retained for the higher Nb compositions, Ti-35Nb and Ti-49Nb. The formation of the martensitic microstructures depends on the content of the β -stabilizing element. For low Nb-content alloys the hexagonal α' -martensite forms and as the Nb-content increases the orthorhombic α'' -martensite transforms³⁰. As illustrated by the microstructures in Fig. 4.6 and XRD analysis in Fig. 4.7 the α' -martensitic structure transformed in the alloys with low Nb content and α'' -martensite in the higher Nb content. The M_s temperature is believed to have decreased as the Nb content increased due to the β -phase being retained and the martensitic phases not fully transforming until the β -phase was fully retained for Ti-35Nb as expected for Ti-Nb alloys^{19,48}.

The initial phases of the alloys transformed into different phases as the alloys were heated from room temperature to temperatures above the β -transus temperature. The transformation that occurred in CP-Ti, Ti-1Nb and Ti-7Nb was the α -phase into the β -phase

transformation from the initial hexagonal α - and α' -phases. There was a different transformation pathway for Ti-(13-35 wt.%) Nb alloys. The initial β -phase transformed into the athermal ω -phase which in turn decomposed into unstable β -phase that immediately transformed into the α -phase. Then the α -phase transformed into the β -phase. There were no detectable phase transformations for Ti-49Nb alloy, the high temperature β -phase was stabilized throughout the increase in temperature.

Table 4.3: The microstructures and phases of the Ti-Nb alloys obtained by OM and XRD analysis and the phase transformations pathways of the alloys.

Alloys (wt.%)	Microstructure-OM	Phases-XRD	Phase transformations-DSC
CP-Ti	α	α	$\alpha \rightarrow \beta$
Ti-1Nb	α	α	$\alpha \rightarrow \beta$
Ti-7Nb	α'	α/α'	$\alpha \rightarrow \beta$
Ti-13Nb	$\alpha'+\alpha''$	$\alpha'+\alpha''+\beta$	$\beta \rightarrow \omega \rightarrow \beta \rightarrow \alpha \rightarrow \beta$
Ti-28Nb	$\alpha'' + \beta$	$\alpha'' + \beta$	$\beta \rightarrow \omega \rightarrow \beta \rightarrow \alpha \rightarrow \beta$
Ti-35Nb	β	β	$\beta \rightarrow \omega \rightarrow \beta \rightarrow \alpha \rightarrow \beta$
Ti-49Nb	β	β	No transformations

4.2.4 Vickers micro-hardness of the as-cast and solution-treated Ti-Nb alloys

The Vickers micro-hardness of the as-cast Ti-Nb alloys was measured to evaluate the effect of Nb content on the microhardness. Figure 4.17 presents micro-hardness versus Nb composition in Ti alloy. The micro-hardness of the as-cast Ti-Nb alloys increased as the Nb content was increased up to 28 wt.% Nb. However, a slight decrease in the hardness was observed after 35 wt.% Nb. The highest micro-hardness of 291.92 Hv_{0.5} was achieved in this study at 28wt%Nb. Whereas, the lowest micro-hardness was obtained at 197.81 Hv_{0.5} for 1 wt.%Nb. The high value of microhardness in Ti-28Nb could be due to the evolution in phases from the α -phase to the α' - and α'' -martensitic phases and β -phase retained in the alloys as Nb content increases. Ti-28Nb alloy which had the highest micro-

hardness had a phase composition of α'' -martensite and β -phase. The decrease occurred for the β -phase alloys Ti-35Nb and Ti-49Nb.

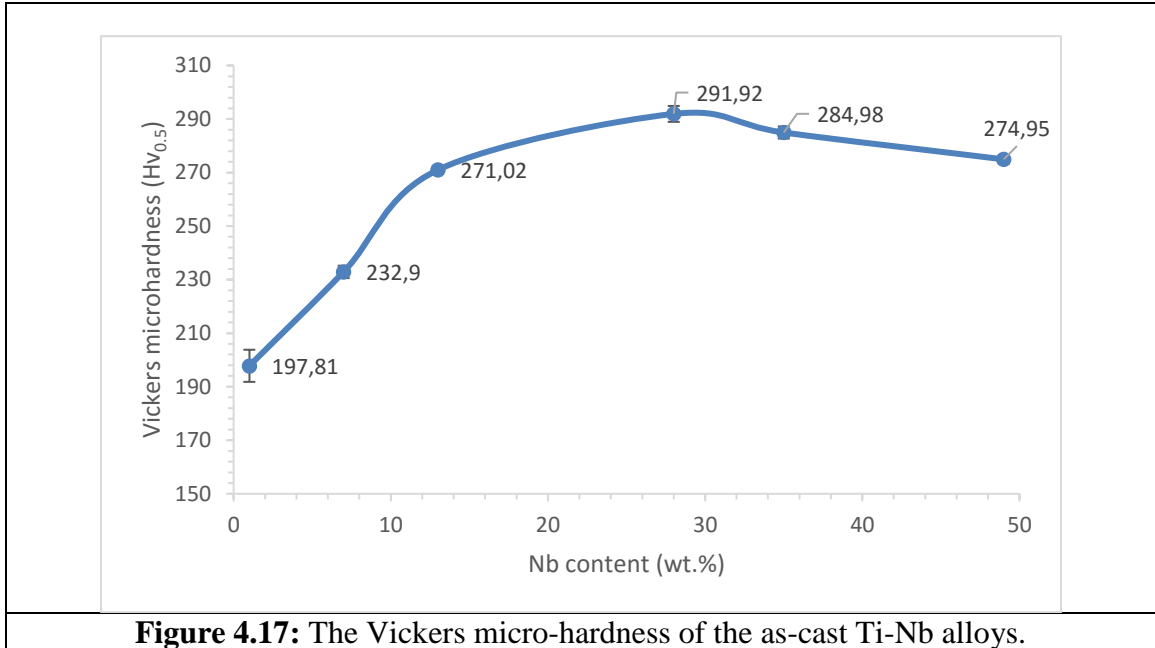


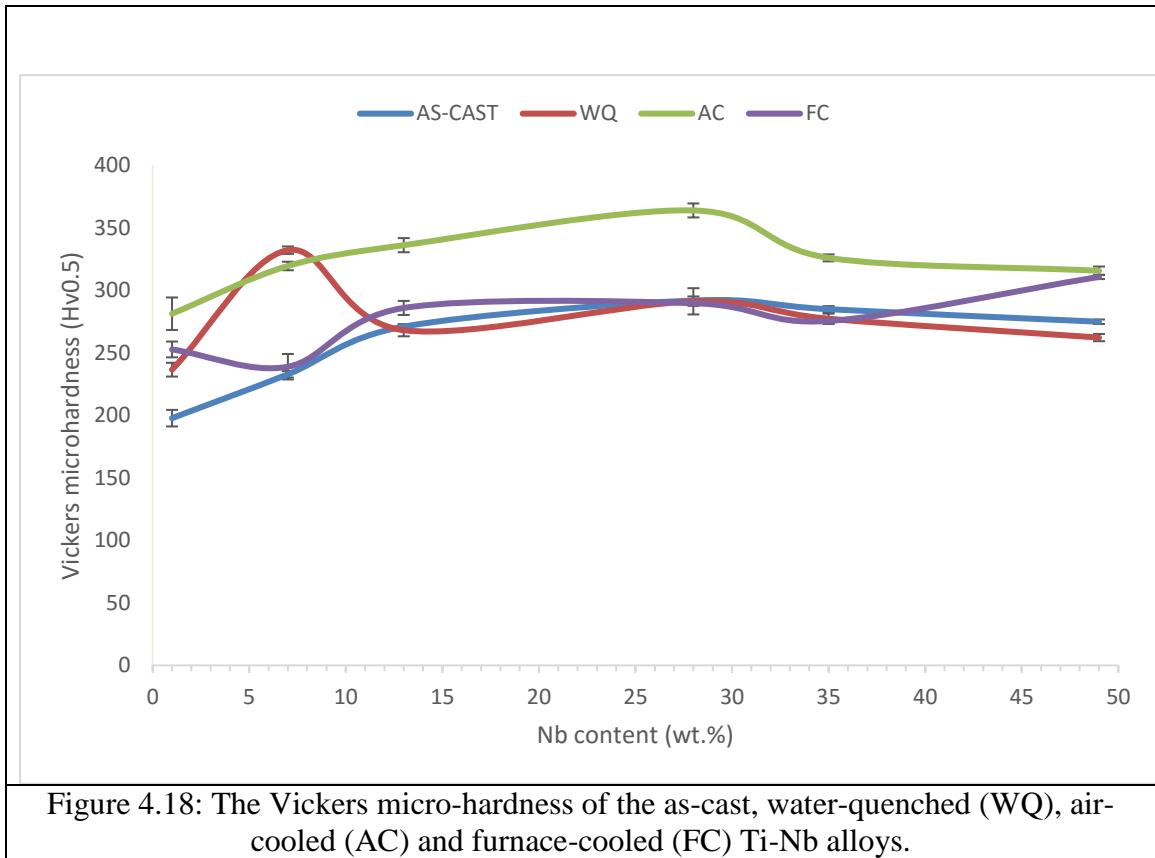
Figure 4.17: The Vickers micro-hardness of the as-cast Ti-Nb alloys.

The Vickers micro-hardness of the as-cast samples and the samples that were solution-treated and cooled in the furnace, air and water are displayed in Fig. 4.18. The microhardness of the solution-treated Ti-Nb alloys was determined to evaluate the effect of different cooling rates on the mechanical properties of the alloys.

The Ti-1Nb alloys microhardness gradually increased from the as-cast alloy to the air-cooled sample which had the highest hardness before it decreased for the furnace-cooled sample. The Ti-1Nb alloy samples all retained the α -phase after solution treatment and were cooled in different cooling mediums. The microhardness of Ti-7Nb alloy increased from the as-cast sample to water-quenched sample which had the highest microhardness for the alloy as the cooling rates changed before it decreased for the air- and furnace-cooled

samples as shown in Fig. 4.18. The difference in micro-hardness of the Ti-7Nb alloy is due to the different microstructures of the samples.

The as-cast and water-quenched samples of Ti-13Nb alloy had similar phase compositions which consisted of the α' - and α'' - martensitic phases and the β -phase as seen in Fig. 4.(a-b); this phase composition exhibited similar microhardness for these samples. The microhardness had a significant increase as the cooling rate decreased from the water-quenched sample to the air-cooled sample before a decrease for the furnace-cooled sample. The Ti-28Nb and Ti-35Nb alloy exhibited the same trend for microhardness as Ti-13Nb alloy as the cooling rate decreased due to the cooling mediums used after solution treatment. The air-cooled samples had the highest micro-hardness for Ti-28Nb and Ti-35Nb alloys. The micro-hardness of Ti-49Nb alloy had a fluctuating trend even though the as-cast sample and the solution treated samples all had fully retained the β -phase. The air- and furnace-cooled samples had significantly higher hardness than the as-cast and water-quenched samples.



The micro-hardness of the alloys varied as the Nb content increased from Ti-1Nb to Ti-49Nb for the as-cast samples and the different cooling rates. There is a general increase in micro-hardness as the Nb content increases before it decreases for the as-cast, water-quenched, air-cooled and furnace-cooled samples. The Ti-28Nb alloy generally had the highest micro-hardness for the as-cast and air-cooled samples except for the water-quenched and furnace-cooled samples where Ti-7Nb and Ti-49Nb alloys had the highest micro-hardness, respectively.

4.2.5 Tensile properties of the as-cast Ti-Nb alloys

The effect of Nb content on the mechanical properties was evaluated by determining the tensile properties of the alloys. The mechanical properties of the alloys depended on the phases present in the alloys with different Nb content. Figure 4.19 illustrates the

engineering stress-strain curve of the Ti-Nb alloys, showing the alloys behavior under stress.

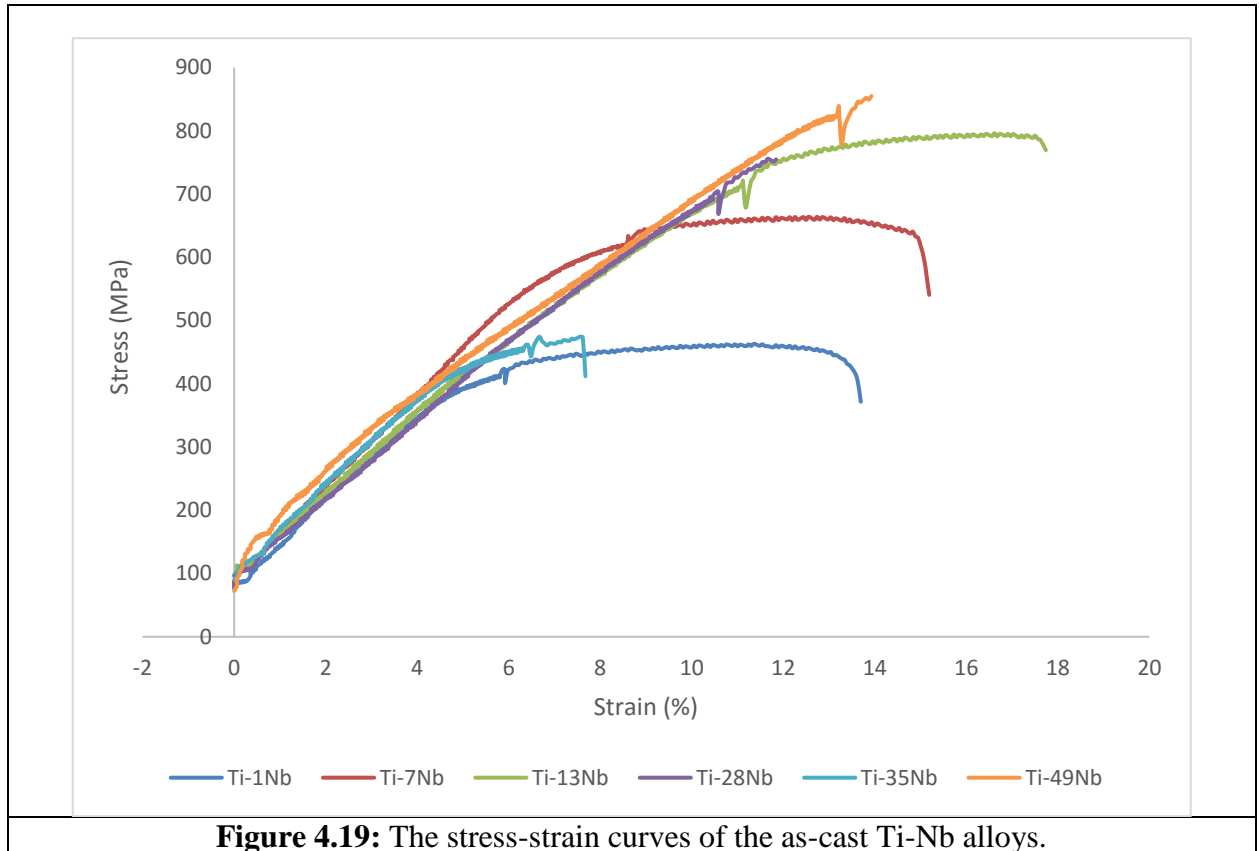


Figure 4.19: The stress-strain curves of the as-cast Ti-Nb alloys.

The tensile properties of the as-cast Ti-Nb alloys have been presented in Fig. 4.20-21. The influence of the Nb content on the ultimate tensile strength and the 0,2% yield strength is shown in Fig. 4.20. The 0.2% yield strength and the ultimate tensile strength of the Ti-Nb alloys both increased as the Nb content increased before there was a decrease from Ti-28Nb alloy. However, Ti-49Nb alloy had the highest yield strength and ultimate tensile strength.

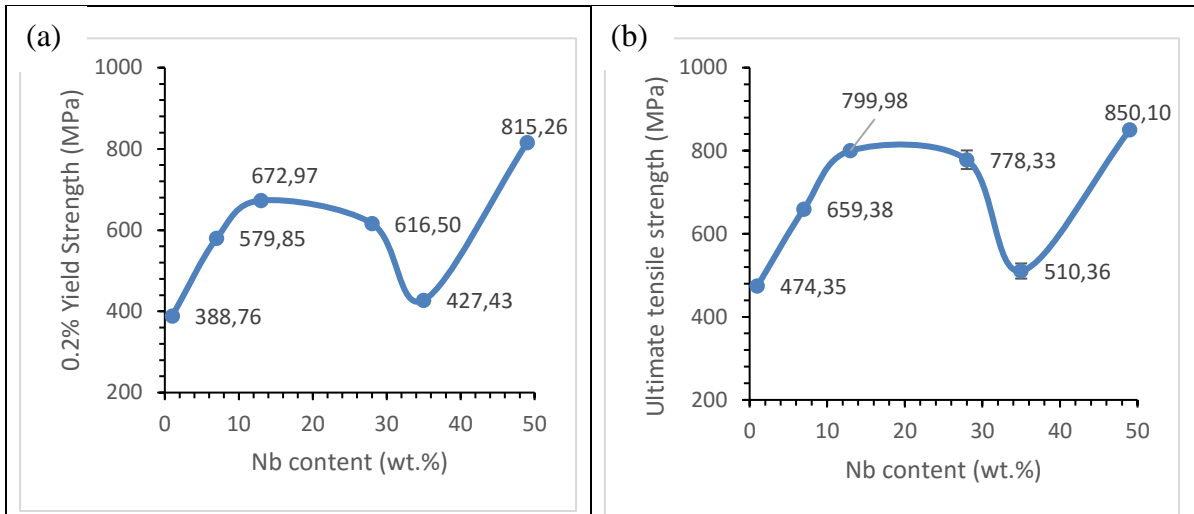
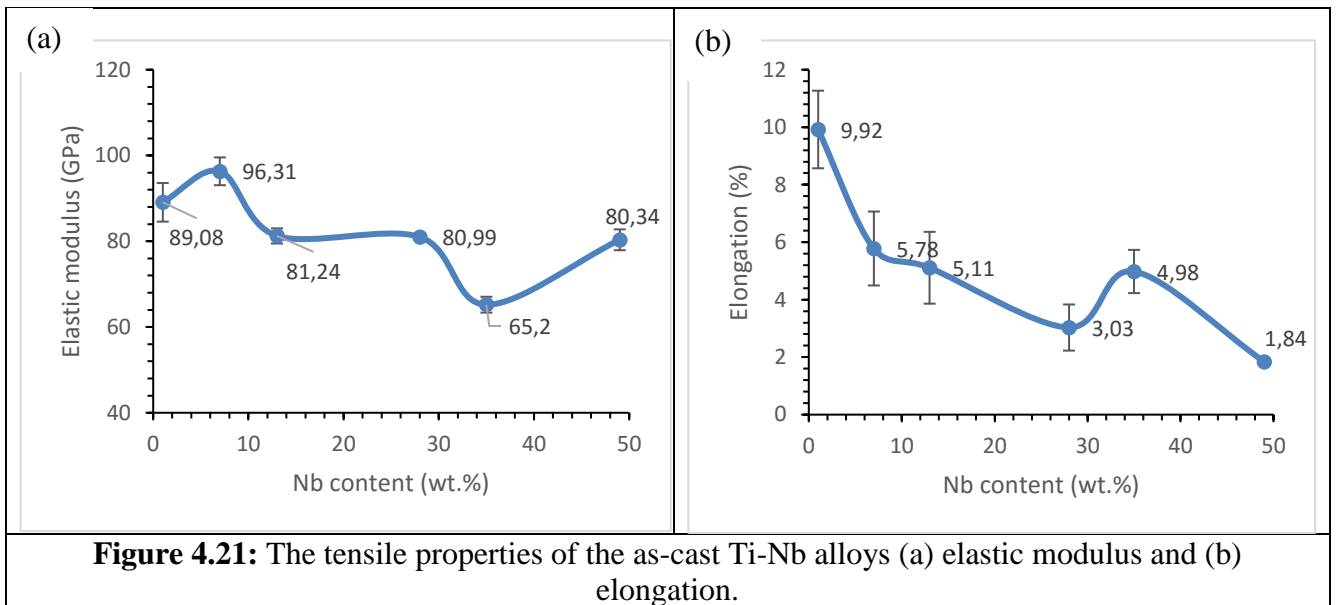


Figure 4.20: The tensile properties of the as-cast Ti-Nb alloys the (a)0.2% yield strength and (b) ultimate tensile strength.

The effect of the Nb content on the Young's modulus and the tensile ductility of the Ti-Nb alloys has been illustrated in Fig. 4.21. The results show that the elastic modulus decreased due to the addition of the Nb as a β -stabilizing element for the Ti-Nb alloys with a range of 65.2 – 96.31 GPa. The elastic modulus as a function of the Nb content exhibited a fluctuating trend due to the phase compositions obtained by the Ti-Nb alloys. The stabilization of the β -phase led to a decrease in the Young's modulus as seen in the Ti-Nb alloys as exhibited in Fig. 4.21. The fully β -phase Ti-35Nb alloy had the lowest Young's modulus of 65.2 GPa. However, Young's modulus of Ti-49Nb increased even though the alloy had fully retained the β -phase. The elongation of the Ti-Nb alloys is illustrated in Figure 4.21(b) shows that the % elongation decreases with increasing Nb content before it increases for Ti-35Nb and then there was a decrease in the Ti-49Nb, which had the lowest elongation of 1.84%. In summary, the modulus of elasticity obtained is in the range of 65.2 – 96.31 GPa the values are relatively lower compared with commonly used bio-metals (Ti-6Al-4V, CP-Ti, stainless steel, Co-Cr-Mo) which ranges from 110 - 200 GPa. The values obtained are highly desirable as they are closer to the modulus of the human bone (10 – 40

GPa) and can promote good osseointegration⁴⁹. Moreover, the yield strength and ultimate tensile strength obtained in the study ranges from 388.76 – 815.26 MPa and 474.35 – 850.10MPa are comparable to the bio-metals values which are 170 – 900 MPa and 465 – 1795MPa, respectively⁴⁹.



CHAPTER 5. DISCUSSION

The microstructural and phase evolution of the alloys due to the influence of the Nb content on the alloys has been discussed here. The discussion on effect of the Nb on the micro-hardness of the Ti-Nb alloys and the effect of the cooling medium on the micro-hardness of the solution-treated alloys. The phase transformations that occurred in the Ti-Nb alloys following thermal analysis is discussed. The effect of the Nb content and phases on the tensile properties of the Ti-Nb alloys are also discussed.

5.1 Characterization of the starting elemental powders

The particle size distribution and particle morphology of the starting powders determined provides an understanding of their influence on the fabrication processes and properties of the alloys. The powder particles of both CP-Ti and Nb had irregular morphology as seen in Fig. 4.1 (c-d). The irregular shape of the CP-Ti particle powder is typical for titanium powders produced using the hydride-dehydride milling process in which the brittle material is crushed to obtain the irregular shape. This has been reported to be suitable for rigid die consolidation⁵⁰. The irregular shape of these starting powder particles has been reported to be ideal for cold compaction because the powder particles are expected to form permanent bonds as they interlock during consolidation⁴⁵. Therefore, the observed morphology of the elemental powder particles was suitable for cold compaction which was done to consolidate the powders before the vacuum arc remelting process for casting.

The oxygen content of the starting powders was determined as oxygen is a major concern when producing titanium alloys. The determined oxygen content of the starting titanium

powder is 0.22 wt.% which is lower than the maximum amount specification for titanium grade 2 of 0.25 wt.% according to the ASTM F6-00 standard. Therefore, the starting titanium powder can be specified as the ASTM grade 2 titanium⁵¹. Oxygen has substantial solubility in titanium as it occupies interstitial sites between titanium ions in the crystal lattice^{15,52}. The dissolving of oxygen atoms in the crystal lattice have an effect on the overall mechanical properties of titanium due to the strain that is created which increases strength whilst decreasing ductility⁵². The oxygen element is classified as an α -stabilizer which means it stabilizes the α -phase at high temperatures thus increasing the β -transus temperature of titanium¹⁵. The phase analysis of CP-Ti showed that it has the hexagonal (HCP) crystal structure as un-alloyed titanium at ambient temperature and pressure is expected to have the HCP crystal structure¹⁵. The alloying element Nb had the cubic (bcc) crystal structure. The Nb element is a β -stabilizer element, when its added to titanium it stabilizes the β -titanium phase at lower temperatures⁵³.

5.2 Characterization of the Ti-Nb alloys

5.2.1 Microstructural analysis of the as-cast and solution-treated Ti-Nb alloys

Alloying titanium with a β -stabilizing element will lead to formation of different metastable phases such as the α' - and α'' -martensite, ω -phase, and the β -phase nucleating after cooling from the β -phase field^{12,54}. The microstructural evolution of the as-cast Ti-Nb alloys is shown in Fig. 4.4. Addition of 1 wt.% Nb in CP-Ti resulted in the formation of the lamellar microstructure which is a secondary α -phase that transforms from the β -phase when cooling from above the β -transus temperature⁵⁵. The as-cast Ti-Nb alloys were cast using water-cooled copper hearth which led to fast cooling of the Ti-Nb alloys. Fast

cooling from the β -phase field of pure Ti and dilute Ti-alloys can result in two different crystal structures of athermal microstructures, the hexagonal α' -martensite and the orthorhombic α'' -martensite^{55,56}. The α' -martensitic microstructure can occur in two different morphologies; the lath type martensite for dilute alloys and the acicular martensite for Ti- alloys with slightly higher alloying element content⁵⁶. Therefore, the increase in the Nb content added to 7wt.% and fast cooling led to the transformation of α - and α' -laths as shown in Fig. 4.4(b). The martensitic microstructures nucleate at a specific temperature as the temperature lowers when cooling from the β -phase field³⁷. The microstructures evolved from the α/α' -laths to the acicular martensite as the Nb content increased to 13wt.%. Similar results in microstructural evolution for Ti-Nb alloys with compositions ranging from 5-15 wt.% were observed in studies^{36,57}. The phase and structure of the martensite in β - stabilized Ti-alloys depends on the amount of the alloying element. It has been reported that the formation of α'' -martensite phase which lowers Young's modulus is preferred over α' -martensite as the Nb content increases.

The high temperature metastable β -phase started nucleating as the Nb content increased to 28wt.% as shown in Fig. 4.4(d). The M_s and M_f temperatures are dependent on the alloying element content, as the alloying element concentration increases they decrease^{15,57}. Therefore, the β -phase being retained in the Ti-28Nb alloy indicates that the M_f temperature had been lowered below room temperature. The β -phase was fully retained as Nb content increased to 35 and 49 wt.%. Both the M_s and M_f temperatures have been lowered below room temperature as the martensitic phases were suppressed from transforming and the β -phase was fully obtained for Ti-35Nb and Ti-49Nb alloys⁵⁷. The retained β -phase for Ti-35Nb and Ti-49Nb alloys is in agreement with the expected Nb

compositions that completely retain stable β -phase which should be at least 35-40 (wt.%)Nb in Ti-Nb alloys²².

The as-cast Ti-Nb alloys were solution-treated above the β -transus temperature in the β -phase field and cooled in the furnace, air, and water. The transformation of the β -phase from the β -phase field can be diffusion-less resulting in martensitic phases forming or be by diffusion controlled nucleation into the equilibrium phases depending on the cooling rate and alloy composition⁴⁵. This shows that the microstructural evolution in the Ti-Nb alloys depends on the content of the Nb content and the cooling rate or the cooling medium used. The cooling rates of the furnace cool, air cool and water quench processes have been determined to be 0.1 °C/s, 4 °C/s and 160 °C/s respectively⁵⁷.

The α -lamellar structures of Ti-1Nb alloy obtained for the different cooling mediums after solution treatment differ in width; with the air-cooled sample having a smaller width than the other samples. The cooling rate from the solution treatment temperature determines the α -lamellar colony size and the width of the α -lamellar as exhibited in Fig. 4.5 for the solution treated samples⁴⁵. The α -lamellar colonies are α -laths and each colony has the same crystallographic variant⁴⁵. The lighter regions or interface between the α -lamellar are Nb-rich regions indicating the presence of the β -phase as shown in Fig. 4.7(a) for the Ti-7Nb furnace-cooled sample. The α -phase starts to nucleate along the β -grain boundaries and grows into the β -grains as the alloys are being cooled below the β -transus temperature as α -phase is incoherent with respect to the β -phase⁴⁵. The α -phase continued to grow in the β -grains and boundaries resulting in colonies of α -lamellar and retained β -matrix as seen in Fig 4.6 and Fig. 4.8. As the cooling rate increased from the furnace-cooled to the air-cooled the colony size and the width of the lamellar decreased⁴⁵. Fast cooling and the

increase in Nb content from Ti-1Nb to Ti-7Nb led to the transformation of the fully acicular martensitic microstructure. The α' -lath type microstructure of the as-cast Ti-7Nb alloy was refined to the acicular α' -martensite as the sample was fast cooled^{1,58}.

The α -phase transformed as α -lamellar microstructures as the Ti-13Nb alloy was furnace cooled and as α -globular grains when air cooled after solution treatment as shown in Fig 4.8 (c-d). The precipitation of the α -phase in the air and furnace-cooled samples occurred through a series of phase transformations as follows, $\alpha'' > \beta > \beta + \omega > \alpha + \beta$ ²². The α'' -martensite in the as-cast sample transformed into the β -phase, in which the ω -phase nucleated before it transformed back into the β -phase as the temperature increased as seen in the DSC results for Ti-13Nb alloy. As the samples cooled from the β -phase field, the α -phase was transformed from the β -phase. The α'' -martensite microstructure is conventionally retained by direct casting from the molten state and by solution treating the alloy in the β -phase field and water quenching the alloy as seen for the as-cast Ti-13Nb microstructure and the heat treated samples⁵⁹. The lighter regions in the furnace-cooled Ti-13Nb sample micrograph between α -lamellar or in the lamellar interfaces in Fig. 4.7-8 are Nb-rich as well as the lighter martensitic-rich regions for the air-cooled sample. The Nb-rich regions in the Ti-Nb alloys as seen in Fig. 4.6-8 are characterized as the β -phase because Nb is β -stabilizer therefore it partitions into the β -phase³⁷. The partitioned Nb content into the untransformed β -phase for the air-cooled sample was however, not enough to lower the M_s temperature below room temperature as the α'' -martensite still transformed within the β -phase. Water quenching of the Ti-13Nb alloy resulted in a martensitic structure transforming within the β -phase matrix. The β -phase is expected to be retained for Ti-Nb alloys with a Nb content above 35 wt.%, as shown for the as-cast and water-

quenched Ti-35Nb and Ti-49Nb alloys^{37,48}. The slow-cooled Ti-35Nb samples had the martensitic phases nucleated and anomalous structures for Ti-49Nb alloy.

The precipitation of the different equilibrium and non-equilibrium phases after the solution treatment were dependent on the cooling rate and Nb content. At slow cooling rates the α -phase nucleation occurred leading to a combination of α and β -phases and at fast cooling rate the martensitic phases transformed at low β -stabilizer content¹⁶. As the Nb content increased, for the slow cooling rates a mixture of the martensitic phase and β -phase were obtained and the β -phase was retained at fast cooling rates.

5.2.2 Phase analysis of the as-cast and solution-treated Ti-Nb alloys

The phase analysis of the Ti-Nb alloys was done by XRD analysis to identify the phases obtained as the Nb content increased. The hexagonal (HCP) crystal structure was identified in both the Ti-1Nb and Ti-7Nb alloys as shown in Fig. 4.12. The α -phase and α' -martensitic phase are difficult to distinguish with XRD analysis as they both have the hexagonal close packed crystal structure with slight differences in the lattice parameters^{59,60}. The α' -martensitic phase crystal structure is called the distorted hexagonal close packed crystal structure. It has been found that when small amounts of a β -stabilizing element are added to titanium, a martensitic structure with the distorted hexagonal crystal structure is obtained⁵⁷. Therefore, the phase obtained for Ti-7Nb was the hexagonal α' -martensitic phase as observed in the microstructure in Fig. 4.4(b). Lee *et al.* (2002)³⁶ observed the α' -martensitic phase for Ti-Nb alloys with 5-10 wt.% Nb content in their study of Ti-Nb alloys, these results were similar to the martensitic microstructure and phase observed for the Ti-7Nb alloy in this study³⁶.

The orthorhombic α'' -phase was detected in the Ti-13Nb alloy through XRD analysis as shown in Fig. 10. This was expected because it had been reported that for Ti-Nb alloys, the α'' -martensitic phase starts transforming for alloys with the composition close to 12wt.%²². The β -phase was also detected in the Ti-13Nb alloy even though it was not observed through metallographic analysis. The presence of the β -phase in the as-cast Ti-13Nb alloy is in agreement with the β -phase found in alloys with low Nb compositions as was found in Ti-10Nb and Ti-15Nb alloys in Ti-Nb studies conducted by Zhang *et al.* (2020)⁴². The splitting of the XRD peaks has also been found to be an indication of the presence of α'' -orthorhombic phase in the alloy as seen in Ti-Nb studies conducted by Lee *et al.* (2002)³⁶. The structure or the phase obtained are influenced by the amount of the alloying element in rapidly cooled β -stabilized Ti-alloys as the Nb content increases the formation of α'' is more preferred than the formation of α' -martensite²⁹.

The β -phase and the α'' -orthorhombic phase were the phases that were detected for the Ti-28Nb alloy. The hexagonal ω -phase has been reported to be found in Ti-Nb alloys with 25-35 wt.% compositions^{33,36}. The athermal ω -phase which is formed by fast cooling in titanium-transitional metal alloys was not detected by XRD and microstructural analysis for the Ti-28Nb alloy, however, it cannot be ruled out due to the experimental detection limits^{29,32,57}. The cubic (bcc) crystal structure was identified in the high Nb content alloys, Ti-35Nb and Ti-49Nb.

The phase evolution occurred as the Ti-Nb alloys were cooled at different cooling rates after solution treatment with increasing Nb content. The as-cast and solution-treated samples of Ti-1Nb alloy exhibited the hexagonal crystal structures as expected as all the samples had the α -lamellar microstructure. The Ti-7Nb alloy as-cast and solution-treated

samples also exhibited the hexagonal crystal structure as shown in Fig. 4.13. The α - and α' -phases both have the hexagonal closed packed crystal structure therefore they cannot be distinguished using XRD analysis, however, they exhibit different microstructures⁵⁹. The α -phase has coarse plate-like microstructures whereas the α' -martensite structure exhibits either lath-type like microstructure or fine acicular microstructure depending on the amount of the alloying element^{56,57}. Therefore, based on the microstructural analysis of the as-cast and water-quenched samples of Ti-7Nb alloy, had the hexagonal α' -martensitic phase. However, the coarse α -lamellar microstructures can be refined depending on the heat treatment and cooling rate as exhibited in Fig. 4.6(c-d) for the furnace- and air-cooled samples for Ti-7Nb alloy. Fast cooling of the as-cast and the water-quenched samples of the Ti-13Nb alloy led to a mixture of the martensitic phases and the β -phase being retained. The splitting of the α/α' peaks is an indication of the presence of the α'' -phase as shown in the XRD patterns of Ti-13Nb alloy in Fig. 4.14⁶⁰. The increase of Nb content to 28wt.% led to increase in β -phase being retained. The β -phase was the predominant phase in the water-quenched Ti-28Nb alloy due to the increase in Nb and the fast cooling of the sample after solution treatment. The martensitic phases transformed in the furnace-cooled sample of the Ti-35Nb alloy and a decrease was seen in their transformation as the cooling rate increased by air-cooling as shown in the XRD patterns in Fig. 4.15. The as-cast and water-quenched samples had fully retained the β -phase.

5.2.3 Thermal analysis of the as-cast Ti-Nb alloys

The phase transformations of the alloys that occur in solid state are very important for determining mechanical properties of the alloys and their behaviour during temperature fluctuations⁴⁵. Thermomechanical processing of alloys can be designed based on these

transformations to obtain the desired mechanical properties depending on the applications of the alloys. The DSC thermal analysis measures the heat flow required to maintain the same temperature for the sample and reference; therefore a change in the heat flow whether endothermic or exothermic indicates a phase transformation in the sample^{61,62}. The CP-Ti had an α -phase to β -phase endothermic transformation, which had a transformation temperature higher than that of pure Ti of about 882 °C¹⁵. Oxygen is an α -stabilizing element and therefore stabilizes the titanium α -phase by increasing the β -transus temperature hence the increase in the transformation temperature¹⁵. The Ti-1Nb and Ti-7Nb alloys both showed the α - to β -phase endothermic transformation which had shifted to lower temperatures as shown in Fig. 4.16(a). The shift in the α - into β -phase transformation peak is due to the increase in the β -stabilizing element as it decreases the β -transus temperature. The phase transformation evolution changed as the Nb content increased to 13-35 wt.%, in addition to the α - into the β -phase transformation other exothermic and endothermic reactions occurred. The initial β -phase of the Ti-13-35Nb alloys transforms into the isothermal ω -phase Fig 4.16(b). The formation of the isothermal ω -phase in Ti-alloys occurs due to aging, which explains the formation of the phase as the Ti-Nb alloys were being heated³². The maximum temperature for the ω -phase stability has been reported to be 484.85 °C in Ti-Nb alloys, therefore the endothermic reaction that occurred around 450 °C is the decomposition of the ω -phase into the β -phase²⁹. The formation of the β -phase was quickly followed by its transformation into the α -phase which in turn transforms into the β -phase.

5.2.4 *Micro-hardness of the as-cast and solution-treated Ti-Nb alloys*

The as-cast Ti-1Nb alloy had the lowest micro-hardness due to the α -phase it obtained which has been found to have the lowest hardness in Ti-Nb alloys, see Figure 4.15^{36,57}. The Ti-13Nb alloy with the α' -, α'' -martensitic phases and β -phase as shown in the XRD pattern in Fig. 4.10 had a higher micro-hardness than the Ti-7Nb alloy which consisted of the α/α' phases. Lee *et al.* (2002)³⁶ reported that the α' -martensite microstructure has a higher micro-hardness than that of the α -phase and α'' -martensitic phase^{36,57}. The higher micro-hardness is due to the high strain involved in the transformation of the α' -martensite as it is a distorted hexagonal crystal structure and this leads to higher work hardening due to the lattice invariant strains^{36,63}. The higher hardness of Ti-13Nb alloy than that of Ti-7Nb was due to the predominant finer acicular α' -martensite present in the alloy compared to the lath-type α' -martensitic microstructure. The increase in Nb content also had an effect on hardness due to the solid solution strengthening effect⁶⁴.

The as-cast Ti-28Nb alloy had the highest microhardness with a phase composition of α'' -martensite and β -phase. The increase in hardness is due to the presence of the ω -phase which has been reported to have the highest hardness even in minute amounts^{36,57}. Thoenmes *et al.* (2019)³³ suggested that the high hardness of Ti-29Nb alloy may be due to the presence of the ω -phase even though they were unable to detect it with XRD analysis⁵⁷. The Ti-28Nb alloy had the highest hardness due to the phase composition of α'' -, β -, ω -phase as found in a similar studies of Ti-Nb alloys with compositions of 25-35Nb wt.% alloys in which the ω -phase was detected to show significant impact on the mechanical properties^{33,36}. The transformation of the hexagonal ω -phase can occur through fast cooling from the β -phase field or during aging of quenched alloys^{32,57}. The hardness of the β -phase

alloys, Ti-35Nb and Ti-49Nb was higher than the alloys with lower Nb content with α - and martensitic phases due to the high amounts of Nb that caused solid solution strengthening effect ⁶⁴. The increase in microhardness of the as-cast Ti-Nb alloys as the Nb content increases before it decreases was due to the phases obtained in the alloys that have different hardening effects.

The different cooling rates led to nucleation of different phase compositions as the Nb content increased for the Ti-Nb alloys after the alloys were solution treated. The as-cast and solution-treated samples of the Ti-1Nb alloy all had the α -lamellar microstructures, however the lamellar structures differed in width and colony size. The size of the α -lamellar colonies, the thickness of the α -lamellar, the β -phase in the lamellar interface and the grain size are very important factors that have an effect on the mechanical properties ⁴⁵. The air-cooled sample had the highest hardness in the Ti-1Nb alloy, and it had smallest lamellar structure width. The furnace-cooled sample of Ti-7Nb alloy had a $\alpha+\beta$ -lamellar microstructure and the as-cast sample had α/α' -laths and these phase compositions exhibited similar hardness. Whereas the water-quenched sample had the highest hardness for Ti-7Nb alloy which consisted of acicular α' -martensite which is known for its high hardness due to the distorted hexagonal crystal structure ³⁶. The high strain involved in the transformation of the distorted hexagonal crystal structure of the α' -martensite leads to lattice invariant strains that causes high work hardening ^{36,63}. The fine acicular α' -martensite structure of the water-quenched sample and the refined α -lamellar microstructures of the air-cooled sample also led to the increase in hardness, as the fine microstructures acted as barriers for the dislocations causing strain in the material.

The air-cooled sample of Ti-13Nb alloy had the highest hardness with a phase composition of α -, α'' -martensite and β -phase. The globular α -phase that transformed in the air-cooled sample has been reported to form in aged water-quenched martensitic samples after heat treatment ^{10,65}. The β -Ti alloys can be strengthened by applying certain heat treatment processes to the alloys which would lead to the transformation of the metastable phases in the α -phase, thus strengthening the alloys ⁴⁶. The precipitation of the α -phase in β -titanium alloys has been reported to increase hardness as seen in the air-cooled Ti-13Nb sample ^{10,66}. The as-cast and water-quenched samples of Ti-13Nb alloy exhibited similar hardness as shown in Fig. 4.17 and these samples both consisted of the martensitic phases and the β -phase. As the cooling rate decreased from air-cooled to the furnace-cooled, the hardness also decreased. The as-cast and water-quenched samples of Ti-28Nb alloy had a phase composition of the α'' - and β -phase whereas the furnace-cooled sample consisted of the α' -, α'' - and β -phase. These samples all exhibited similar hardness as shown in Fig 4.17, due to the similar phase compositions. The air-cooled sample retained a fully α'' -martensitic phase which had the highest hardness for Ti-28Nb alloy. The finer acicular α'' -martensitic microstructure and the inter-granular grains led to the high hardness for the water-quenched sample of Ti-28Nb alloy ¹⁰.

The air-cooled sample of Ti-35Nb alloy had the highest micro-hardness with a phase composition of the α'' - and β -phase. The small amounts of the α'' -phase detected in Ti-35Nb air-cooled sample by XRD analysis as shown in Fig. 4.15 had a huge impact on the hardness of the alloy as the hardness increased significantly from the water-quenched sample. The micro-hardness of Ti-49Nb alloy samples fluctuated even though the samples all had fully retained the β -phase. The higher hardness maybe due to the anomalies in the

microstructures of the air- and furnace-cooled samples of Ti-49Nb alloy as shown in Fig. 4.10(c-d).

The hardness generally increased due to the evolution of the phases present in the different alloys as the Nb content increases which evolved from the α -phase present in Ti-1Nb alloy to a mixture of equilibrium and non-equilibrium phases in the alloys before a general decrease as the β -phase was being retained and finally the fully β -phase in Ti-49Nb alloy. Cardoso *et al.* (2014)⁴⁶ studied the Ti-Mo alloys, the microhardness of the alloys that were water-quenched after heat treatment exhibited a general increase in hardness as the Mo content increased before it decreased for the β -stabilized alloys⁴⁶. The air-cooled samples generally had the highest microhardness for the alloys whereas the as-cast samples had lowest microhardness for the Ti-Nb alloys. Majumdar and Chakraborty in their study of Ti-13Zr-13Nb found that the hardness of the air-cooled samples was higher than that of the furnace-cooled and water-quenched samples for all the samples heat-treated at different temperatures¹⁰. Majumdar and Chakraborty proposed that the higher hardness of the air-cooled samples was due to the finer microstructures obtained¹⁰. This is evident in the microstructures obtained for the Ti-Nb alloys in this study. The α -lamellar microstructure of Ti-1Nb had the smallest lamellar width and the air-cooled samples of Ti-7Nb Ti-13Nb, Ti-28Nb and Ti-35Nb all had finer acicular martensite. The micro-hardness of Ti-Nb alloys has been reported to increase with increasing cooling rate, however for the Ti-Nb alloys in this study it has been exhibited that the micro-hardness does increase from furnace cooling to air cooling before it decreases for the water-quenched samples³⁵.

5.2.5 Tensile properties of the as-cast Ti-Nb alloys

The mechanical properties of Ti-alloys depend on the content of the alloying element, thermomechanical processing conditions and the mechanical behavior of the mixture of the phases in the alloys ⁴⁵. The influence of the Nb content on the tensile properties of the Ti-Nb alloys is illustrated in Fig. 4.20-21. The UTS and 0.2% yield strength of the Ti-Nb alloys increased as the Nb content increased, as compared to before when they decreased as the β -phase was being retained. In contrast, a fully β -phase alloy Ti-49Nb had the highest strengths. Ti-1Nb has an α -phase with the lowest tensile strength of 474.35 MPa and the Ti-35Nb alloy has a β -phase with a lower tensile strength and yield strength compared to the alloys with the mixture of martensitic and β -phases. Zhang *et al.* (2019, 2020)^{22,67} reported an increase in both ultimate tensile strength and yield strength as the Nb content increases from 5-25wt% compared to CP-Ti ¹⁹. The increase in the tensile properties for Ti-(7-28wt%)Nb alloys than that of CP-Ti show that the tensile properties can be enhanced by adding small amounts of Nb ²². The Ti-49Nb alloy exhibited high strength due to the high Nb content.

Young's modulus of the as-cast Ti-Nb alloys as a function of the β -stabilizing Nb content is shown in Fig. 4.19(a). The crystal structure of the material affects the elastic modulus the most, therefore in a multiphase alloy, it is influenced by the phases and their volume fractions ^{10,62}. The variation in elastic moduli of the Ti-Nb alloys as the Nb content increases reflects the effect of the equilibrium and non-equilibrium phases that were formed during the manufacturing process ²². There was an increase in Young's modulus as the Nb content increased from 1 wt.% to 7 wt.%. The elastic modulus decreased to 65.2 GPa for Ti-35Nb alloy and thereafter there was an increase for Ti-49Nb alloy of the as-cast

Ti-Nb alloys The Young's modulus varies depending on the composition of the martensitic phases, ω -phase and β -phase; with β -phase having the lowest Young's modulus for titanium alloys^{7,68}. The increase in Young's modulus for Ti-7Nb before it decreased for Ti-13Nb alloy, has a similar pattern observed in a study by Da Silva *et al.* (2012)²¹ in Ti-5Nb and Ti-10Nb alloys which also exhibited similar microstructures as Ti-7Nb and Ti-13Nb¹⁹. The as-cast Ti-35Nb alloy had fully retained the β -phase and it had the lowest Young's modulus. There was no significant decrease in elastic modulus as the Nb content increased from 13wt% to 28wt% although the alloys exhibited different ratios of the phase compositions. The β -phase present in Ti-28Nb alloy has been reported to have lower Young's modulus than the martensitic phases; however the presence of the ω -phase in the alloy has a significant influence on Young's modulus^{7,36}. Lee *et al.* (2002)³⁶ reported the presence of the ω -phase in Ti-Nb alloys with the composition of 27.5 to 30 wt.% Nb which had increased Young's modulus, the ω -phase is known to increase the Young's modulus due to its hard and dense characteristics^{34,36}. The Ti-35Nb alloy had the lowest Young's modulus of 65.2 GPa. The Ti-35Nb alloy had fully retained the β -phase as shown by the XRD analysis in Fig. 4.10, therefore as expected the β -phase has significantly lowered Young's modulus. Ti-Nb alloys studies conducted by Kim *et al.* (2004, 2006)^{61,69} exhibited a similar behavior in Young's modulus as there was an increase for Ti-40Nb alloy from Ti-30Nb alloy⁷⁰. The increase in Young's modulus may be due to the large content of Nb in the alloy which would cause variations in crystalline structure dimensions thus affecting the Young's modulus⁷¹. The increase in Nb content (β -stabilizing element) led to an increase in the stabilization of the β -phase until the phase was fully stabilized causing the Young's modulus to decrease⁷².

The alloy with the lowest Nb content had the highest ductility before it decreased as the Nb content increased. The ω -phase has been reported to increase the mechanical strength of the material, however it also causes severe brittleness in the material, hence the low ductility for the Ti-28Nb alloy^{30,46,65}. Ti-49Nb alloy had the highest 0.2% yield strength of 815.26 MPa however it had the lowest ductility exhibiting a strong but brittle behavior for the material.

CHAPTER 6. CONCLUSIONS AND RECOMMENDATIONS

The conclusions were drawn from the evaluation of the microstructural evolution of the Ti-Nb alloys due to the Nb content and its effect on the mechanical properties of the alloys. The effect of solution treatment conditions and the use on Ti-Nb alloys was evaluated and conclusions made based on the structures and phases formed and their influence on mechanical properties of the alloys. Recommendations of the experimental work to be done for the study have been given.

6.1 Conclusions

The effect of β -stabilizing element Nb on the microstructural evolution and the mechanical properties of Ti-Nb alloys with varied Nb content was investigated. Based on the results obtained, the following summarized conclusions are made from the study:

- Microstructure evolution with increasing Nb content on as-cast Ti-Nb alloys showed phases transforming from α -lamellar to mixtures of α' - and α'' -martensitic structures and β -phase until fully β -phase was retained. Ti-1Nb alloy was characterized with α -phase, increasing Nb content to 7 wt. % the α -phase transformed into the α' -martensitic phase. Further Nb content increase to 13 and 28 wt.% the α' -martensitic phases and metastable β -phase were obtained. At higher Nb contents of 35 and 49 wt.%, the martensitic phases were suppressed, and metastable β -phase was fully retained.
- Different heat treatments methods that include furnace cooling, water quenching and air cooling were carried out on the Ti-Nb alloys with varied compositions. The different cooling mediums did not alter the α -phase formed on Ti-1Nb alloy.

Furnace cooling transformed martensitic phases into α -phase for Ti-7Nb and Ti-13Nb alloys. For higher Nb contents in Ti-28Nb and Ti-35Nb alloys α' - and α'' -martensite as well as the metastable β -phase were formed. The 35 wt.% Nb did not suppress the formation of the martensitic phases and fully retain the β -phase when the alloy was slow cooled. The Ti-49Nb alloy fully retained the β -phase, however there were anomalous structures that were formed for the furnace and air-cooled samples despite the high Nb content.

Air-cooling Ti-Nb alloys refined the α -lamellar microstructures in width and colony size for Ti-1Nb and Ti- 7Nb alloys. The increase in cooling rate led to the precipitation of α'' -martensite within the retained β -phase and α -globular grains for Ti-13Nb alloy. The α'' -martensitic microstructure fully transformed for the Ti-28Nb alloy when it was air-cooled. Whereas the Ti-35Nb alloy retained the metastable β -phase with α'' -martensite inside the grains.

Water quenching Ti-Nb alloys led to the precipitation of martensitic phases and the β -phase being retained. As the Nb content increased the Ti-13Nb and Ti-28Nb alloys retained the metastable β -phase with α'' -martensite within the β -phase matrix. The high Nb content alloys, Ti-35Nb and Ti-49Nb, fully retained the β -phase when water quenched.

In summary, furnace cooling Ti-Nb alloys after solution treatment above the beta-transus temperature led to the formation of the α -phase at low Nb content and the transformation of the martensitic phases for high Nb content alloys. Increasing the cooling rate by air-cooling led to the refinement of the microstructures and an increase in the β -phase being retained for high Nb content alloys. Water quenching the Ti-Nb alloys led to the decrease in the precipitation of the α -phase and the martensitic phases and an increase in the β -phase

being retained. The β -phase was fully retained for Ti-35Nb and Ti-49Nb. The fast cooling of Ti-Nb alloys is ideal for retaining the β -phase after solution treatment above the beta-transus temperature.

- The phases formed in the as-cast Ti-Nb alloys due to the variation of the Nb content had a significant effect on the mechanical properties of the alloys. The micro-hardness of the alloys increased reaching a peak in the Ti-28Nb alloy, where the phases evolved from the α -phase into martensitic and β -phases. A decrease in hardness was observed as the β -phase was fully retained at higher Nb contents. The refined α -lamellar and martensitic structures for air-cooled samples resulted in highest hardness values among the as-cast, furnace-cooled and water-quenched samples. For water quenched samples the retained β -phase was responsible for low hardness values
- The ultimate tensile strength and 0.2% yield strength also increased as the Nb content increased but decreased as the meta-stable β -phase was being retained for Ti-35Nb alloy. However, there was significant increase of UTS and 0.2% YS increase for Ti-49Nb alloy.
- As-cast Ti-Nb alloys elongation decreased as the Nb content increased until Ti-35wt%Nb alloy when it decreased. The Ti-35Nb alloy characterized with β - phase resulted in the lowest Young's modulus of 65.2 GPa, the fully β -phase Ti-49Nb alloy had increase in elastic modulus due to the high Nb content in the alloy.

6.2. Recommendations

From the results obtained, Ti-35Nb alloy containing β -phase exhibited lowest Young's modulus of 65.2GPa which is relatively closer to that of human cortical bone. As such, Ti-

35Nb alloy is a candidate material for use in biomedical implants. Moreover, water quenching eliminates formation of martensite structures and favours retention of β -phase, in contrast to other heat treatments. β -phase was the dominant phase in water quenching and it is highly attractive for bio-materials.

The following activities are suggested as recommended work to be done:

- For comparison of the Young's modulus of bone to that of the Ti-Nb alloys the determination of the Young's modulus using either resonant ultrasound spectroscopy (RUS) or Impulse excitation (IE) is recommended.
- Biocompatibility tests of the Ti-Nb alloys using cell cultures to evaluate cell growth and adhesion.
- Corrosion tests of the Ti-Nb alloys in simulated body fluids.
- Tensile tests for the solution treated Ti-Nb alloys to study the effect of the cooling mediums on the tensile properties.

REFERENCES

1. Geetha, M., Singh, A. K., Asokamani, R. & Gogia, A. K. Ti based biomaterials, the ultimate choice for orthopaedic implants - A review. *Prog. Mater. Sci.* **54**, 397–425 (2009).
2. Niinomi, M., Nakai, M. & Hieda, J. Development of new metallic alloys for biomedical applications. *Acta Biomaterialia* vol. 8 3888–3903 (2012).
3. Bai, Y. *et al.* Characterization, corrosion behavior, cellular response and in vivo bone tissue compatibility of titanium-niobium alloy with low Young's modulus. *Mater. Sci. Eng. C* **59**, (2016).
4. Chen, Q. & Thouas, G. A. Metallic implant biomaterials. *Materials Science and Engineering R: Reports* vol. 87 (2015).
5. Head, W. C., Bauk, D. J. & Emerson, R. H. Titanium as the material of choice for cementless femoral components in total hip arthroplasty. in *Clinical Orthopaedics and Related Research* (1995).
6. Long, M. & Rack, H. J. Titanium alloys in total joint replacement - A materials science perspective. *Biomaterials* **19**, 1621–1639 (1998).
7. Abdel-Hady Gepreel, M. & Niinomi, M. Biocompatibility of Ti-alloys for long-term implantation. *Journal of the Mechanical Behavior of Biomedical Materials* vol. 20 (2013).
8. Eisenbarth, E., Velten, D., Müller, M., Thull, R. & Breme, J. Biocompatibility of β -stabilizing elements of titanium alloys. *Biomaterials* **25**, (2004).
9. Niinomi, M. Recent research and development in titanium alloys for biomedical applications and healthcare goods. *Science and Technology of Advanced Materials* vol. 4 (2003).
10. Majumdar, P., Singh, S. B. & Chakraborty, M. The role of heat treatment on microstructure and mechanical properties of Ti-13Zr-13Nb alloy for biomedical load bearing applications. *J. Mech. Behav. Biomed. Mater.* **4**, 1132–1144 (2011).

11. Gutiérrez Moreno, J. J. *et al.* Ab-initio and experimental study of phase stability of Ti-Nb alloys. *J. Alloys Compd.* **696**, (2017).
12. Karre, R., Niranjana, M. K. & Dey, S. R. First principles theoretical investigations of low Young's modulus beta Ti-Nb and Ti-Nb-Zr alloys compositions for biomedical applications. *Mater. Sci. Eng. C* **50**, 52–58 (2015).
13. Zhao, D. *et al.* Microstructure and mechanical behavior of metal injection molded Ti-Nb binary alloys as biomedical material. *J. Mech. Behav. Biomed. Mater.* **28**, (2013).
14. Liu, X., Chu, P. K. & Ding, C. Surface modification of titanium, titanium alloys, and related materials for biomedical applications. *Mater. Sci. Eng. R Reports* **47**, 49–121 (2004).
15. Bhadeshia, H. K. D. H. Titanium & its Alloys Pure. *Mater. Sci. Metall.* 1–13 (2005).
16. Cremasco, A. *et al.* Correlations between aging heat treatment, ω phase precipitation and mechanical properties of a cast Ti–Nb alloy. *Mater. Des.* **32**, 2387–2390 (2011).
17. Niinomi, M. Mechanical properties of biomedical titanium alloys. *Mater. Sci. Eng. A* **243**, 231–236 (1998).
18. Maietta, S. *et al.* A further analysis on Ti6Al4V lattice structures manufactured by selective laser melting. *J. Healthc. Eng.* **2019**, (2019).
19. Zhang, Y., Sun, D., Cheng, J., Tsoi, J. K. H. & Chen, J. Mechanical and biological properties of Ti–(0–25 wt%)Nb alloys for biomedical implants application. *Regen. Biomater.* **7**, 119–127 (2020).
20. Schmidt, R. *et al.* Electrochemical deposition of hydroxyapatite on beta-Ti-40Nb. *Surf. Coatings Technol.* **294**, (2016).
21. Da Silva, L. M., Alves Claro, A. P. R., Buzalaf, M. A. R. & Grandini, C. R. Influence of the substitutional solute on the mechanical properties of Ti-Nb Binary Alloys for Biomedical Use. *Mater. Res.* **15**, (2012).
22. Zhang, Y., Sun, D., Cheng, J., Tsoi, J. K. H. & Chen, J. Mechanical and biological

- properties of Ti-(0-25 wt%)Nb alloys for biomedical implants application. *Regen. Biomater.* **7**, 119–127 (2020).
23. Yılmaz, E., Gökçe, A., Fındık, F. & Gülsoy, H. Ö. Electrochemical Corrosion Behavior of Ti and Ti-16Nb Alloy for Implant Applications. *8th Int. Adv. Technol. Symp.* **8**, 2244–2251 (2017).
 24. Bönisch, M. *et al.* Composition-dependent magnitude of atomic shuffles in Ti–Nb martensites. *J. Appl. Crystallogr.* **47**, 1374–1379 (2014).
 25. Moffat, D. L. & Kattner, U. R. Stable and metastable Ti-Nb phase diagrams. *Metall. Trans. A, Phys. Metall. Mater. Sci.* **19 A**, 2389–2397 (1988).
 26. Zhang, Y., Liu, H. & Jin, Z. Thermodynamic assessment of the Nb-Ti system. *Calphad Comput. Coupling Phase Diagrams Thermochem.* **25**, (2001).
 27. Murray, J. L. The Nb-Ti (Niobium-Titanium) system. *Bull. Alloy Phase Diagrams* **2**, (1981).
 28. Kim, H. Y., Satoru, H., Kim, J. Il, Hosoda, H. & Miyazaki, S. Mechanical properties and shape memory behavior of Ti-Nb alloys. in *Materials Transactions* vol. 45 (2004).
 29. Bönisch, M. *et al.* Thermal stability and phase transformations of martensitic Ti–Nb alloys. *Sci. Technol. Adv. Mater.* **14**, 055004 (2013).
 30. Lopes, E. S. N., Cremasco, A., Afonso, C. R. M. & Caram, R. Effects of double aging heat treatment on the microstructure, Vickers hardness and elastic modulus of Ti–Nb alloys. *Mater. Charact.* **62**, 673–680 (2011).
 31. Tobe, H. *et al.* Effect of Nb content on deformation behavior and shape memory properties of Ti–Nb alloys. *J. Alloys Compd.* **577**, S435–S438 (2013).
 32. Kikuchi, M., Takahashi, M. & Okuno, O. Mechanical properties and grindability of dental cast Ti-Nb alloys. *Dent. Mater. J.* **22**, (2003).
 33. Thoemmes, A., Ivanov, I. V., Ruktuev, A. A., Lazurenko, D. V. & Bataev, I. A. Structure and Phase Composition of Biomedical Alloys of the Ti – Nb System in

Cast Condition and After Heat Treatment. *Met. Sci. Heat Treat.* **60**, (2019).

34. Kim, H. Y., Ikehara, Y., Kim, J. I., Hosoda, H. & Miyazaki, S. Martensitic transformation, shape memory effect and superelasticity of Ti-Nb binary alloys. *Acta Mater.* **54**, (2006).
35. Afonso, C. R. M., Aleixo, G. T., Ramirez, A. J. & Caram, R. Influence of cooling rate on microstructure of Ti-Nb alloy for orthopedic implants. *Mater. Sci. Eng. C* **27**, 908–913 (2007).
36. Lee, C. M., Ju, C. P. & Chern Lin, J. H. Structure-property relationship of cast Ti-Nb alloys. *J. Oral Rehabil.* **29**, (2002).
37. Hon, Y. H., Wang, J. Y. & Pan, Y. N. Composition/phase structure and properties of titanium-niobium alloys. *Mater. Trans.* **44**, 2384–2390 (2003).
38. Kim, S. E. *et al.* Elastic modulus and in vitro biocompatibility of Ti-xNb and Ti-xTa alloys. *Met. Mater. Int.* **13**, (2007).
39. Atwood, R. C., Lee, P. D., Minisandram, R. S. & Jones, R. M. F. Multiscale modelling of microstructure formation during vacuum arc remelting of titanium 6-4. in *Journal of Materials Science* vol. 39 (2004).
40. Woodside, C. R., King, P. E. & Nordlund, C. Arc distribution during the vacuum arc remelting of Ti-6Al-4V. *Metall. Mater. Trans. B Process Metall. Mater. Process. Sci.* **44**, (2013).
41. Chapelle, P. *et al.* Characterization of the behaviour of the electric arc during VAR of a Ti alloy. in *IOP Conference Series: Materials Science and Engineering* vol. 143 (2016).
42. Mitchell, A. Solidification in remelting processes. *Mater. Sci. Eng. A* **413–414**, (2005).
43. Sankar, M., Satya Prasad, V. V., Baligidad, R. G. & Gokhale, A. A. Effect of vacuum arc remelting and processing parameters on structure and properties of high purity niobium. *Int. J. Refract. Met. Hard Mater.* **50**, (2015).

44. Kelkar, K. M., Patankar, S. V, Mitchell, A., Kanou, O. & Fukada, N. Computational Modeling of the Vacuum Arc Remelting (VAR) Process Used for the Production of Ingots of Titanium Alloys. *Vacuum* (2003).
45. Tarzimoghadam, Z., Sandlöbes, S., Pradeep, K. G. & Raabe, D. Microstructure design and mechanical properties in a near- α Ti-4Mo alloy. *Acta Mater.* **97**, (2015).
46. Cardoso, F. F., Ferrandini, P. L., Lopes, E. S. N., Cremasco, A. & Caram, R. Ti-Mo alloys employed as biomaterials: Effects of composition and aging heat treatment on microstructure and mechanical behavior. *J. Mech. Behav. Biomed. Mater.* **32**, (2014).
47. Zheng, P. *et al.* On the standards and practices for miniaturized tensile test – A review. *Fusion Eng. Des.* **161**, (2020).
48. Sun, F. *et al.* A thermo-mechanical treatment to improve the superelastic performances of biomedical Ti-26Nb and Ti-20Nb-6Zr (at.%) alloys. *J. Mech. Behav. Biomed. Mater.* **4**, (2011).
49. Nag, S. & Banerjee, R. Fundamentals of Medical Implant Materials. *Mater. Med. Devices* 6–17 (2012) doi:10.31399/ASM.HB.V23.A0005682.
50. Bolzoni, L., Esteban, P. G., Ruiz-Navas, E. M. & Gordo, E. Influence of powder characteristics on sintering behaviour and properties of PM Ti alloys produced from prealloyed powder and master alloy. *Powder Metall.* **54**, (2011).
51. ASTM F67. Standard specification for unalloyed titanium, for surgical implant applications. *ASTM Int.* (2006).
52. McCracken, M. Dental implant materials: Commercially pure titanium and titanium alloys. *J. Prosthodont.* **8**, (1999).
53. de Araujo-Silva, R. *et al.* Synthesis of B-Ti-Nb alloys from elemental powders by high-energy ball milling and their hydrogenation features. *Int. J. Hydrogen Energy* **43**, (2018).
54. Niinomi, M. Mechanical biocompatibilities of titanium alloys for biomedical applications. *Journal of the Mechanical Behavior of Biomedical Materials* vol. 1 (2008).

55. Gammon, L. M. *et al.* Metallography and Microstructures of Titanium and Its Alloys. *Metallogr. Microstruct.* 899–917 (2004) doi:10.31399/ASM.HB.V09.A0003779.
56. Lutjering, G., Williams, J. C. & Gysler, A. Chapter 1 MICROSTRUCTURE AND MECHANICAL PROPERTIES OF TITANIUM ALLOYS.
57. Thoemmes, A., Bataev, I. A., Belousova, N. S. & Lazurenko, D. V. Microstructure and mechanical properties of binary Ti-Nb alloys for application in medicine. *Proc. - 2016 11th Int. Forum Strateg. Technol. IFOST 2016* 26–29 (2017) doi:10.1109/IFOST.2016.7884101.
58. Rack, H. J. & Qazi, J. I. Titanium alloys for biomedical applications. *Mater. Sci. Eng. C* **26**, (2006).
59. Peng, Y. P., Ju, C. P. & Chern Lin, J. H. Effect of heat treatment within alpha/beta dual-phase field on the structure and tensile properties of binary TiMo alloys. *Mater. Trans.* **59**, (2018).
60. Yan, Q. *et al.* Comparison study on microstructure and mechanical properties of Ti-6Al-4V alloys fabricated by powder-based selective-laser-melting and sintering methods. *Mater. Charact.* **164**, 110358 (2020).
61. Arvelakis, S., Jensen, P. A. & Dam-Johansen, K. Simultaneous thermal analysis (STA) on ash from high-alkali biomass. *Energy and Fuels* **18**, (2004).
62. Homporová P. , Maria Cecilia Poletti, M. Stockinger, F. W. Dynamic phase evolution in titanium alloy Ti-6Al-4V — Graz University of Technology. <https://graz.pure.elsevier.com/en/publications/dynamic-phase-evolution-in-titanium-alloy-ti-6al-4v> (2011).
63. Davis, R., Flower, H. M. & West, D. R. F. Martensitic transformations in Ti-Mo alloys. *J. Mater. Sci.* **14**, 712–722 (1979).
64. Han, M.-K., Kim, J.-Y., Hwang, M.-J., Song, H.-J. & Park, Y.-J. Effect of Nb on the Microstructure, Mechanical Properties, Corrosion Behavior, and Cytotoxicity of Ti-Nb Alloys. *Materials (Basel)*. **8**, 5986–6003 (2015).
65. Cremasco, A. *et al.* Correlations between aging heat treatment, ω phase precipitation

- and mechanical properties of a cast Ti-Nb alloy. *Mater. Des.* **32**, 2387–2390 (2011).
66. Ikeda, M., Komatsu, S.-Y., Sowa, I. & Niinomi, M. Aging behavior of the Ti-29Nb-13Ta-4.6Zr new beta alloy for medical implants. *Metall. Mater. Trans. A* **33**, (2002).
 67. Zhang, L. C. & Chen, L. Y. A Review on Biomedical Titanium Alloys: Recent Progress and Prospect. *Adv. Eng. Mater.* **21**, 1–29 (2019).
 68. Bönisch, M. *et al.* Thermal stability and latent heat of Nb-rich martensitic Ti-Nb alloys. *J. Alloys Compd.* **697**, (2017).
 69. Kim, H. Y., Kim, J. I., Inamura, T., Hosoda, H. & Miyazaki, S. Effect of thermo-mechanical treatment on mechanical properties and shape memory behavior of Ti-(26–28)at.% Nb alloys. *Mater. Sci. Eng. A* **438–440**, 839–843 (2006).
 70. Wen, M., Wen, C., Hodgson, P. & Li, Y. Fabrication of Ti-Nb-Ag alloy via powder metallurgy for biomedical applications. *Mater. Des.* **56**, (2014).
 71. Aleixo, G. T., Afonso, C. R. M., Coelho, A. A. & Caram, R. Effects of omega phase on elastic modulus of Ti-Nb alloys as a function of composition and cooling rate. *Solid State Phenom.* **138**, 393–398 (2008).
 72. Zhou, Y. L. & Luo, D. M. Microstructures and mechanical properties of Ti-Mo alloys cold-rolled and heat treated. *Mater. Charact.* **62**, (2011).